Available online at www.sciencedirect.com
SCIENCE DIRECT®
Computer Networks 50 (2006) 2676–2712
Computer Networks
www.elsevier.com/locate/comnet

# A framework and source model for design and evaluation of Robust Header Compression

Chia Yuan Cho [a,*], Winston Khoon Guan Seah [b], Yong Huat Chew [b]

[a] DSO National Laboratories, Information Division, 20 Science Park Drive, Singapore 118230, Singapore
[b] Institute for Infocomm Research, 21 Heng Mui Keng Terrace, Singapore 119613, Singapore

Received 12 December 2004; received in revised form 25 July 2005; accepted 26 September 2005
Available online 17 November 2005

Responsible Editor: X.S. Shen

**Abstract**

Robust Header Compression (ROHC) is a specification being developed by the Internet Engineering Task Force (IETF) for compressing protocol headers robustly over wireless channels to improve bandwidth efficiency. Traditionally, header compression schemes are designed based on qualitative descriptions of source headers. This is inadequate because qualitative descriptions do not precisely describe the effect of different source and deployment scenarios, and it is difficult to perform optimization using this methodology. In addition, due to the use of qualitative descriptions, most studies on header compression performance do not take into account the tradeoff between performance metrics such as robustness and compression efficiency. In this paper, we present a modeling framework for header compression. For the first time, a source model is developed to study header compression. Modeling the way packets are generated from a source with multiple concurrent flows, the source model captures the real-world behavior of the IP Identification header field. By varying the parameters in the source and channel models of our framework, different source and deployment scenarios can be modeled. We use the framework to define and establish the relationship between performance metrics, offering new perspectives to their current definitions. We then introduce the objective of scheme design and the notion of optimal schemes. Based on this new paradigm, we present a novel way to study the tradeoff dependencies between performance metrics. We demonstrate how a scheme can be designed to optimize tradeoffs based on the desired level of performance.


*Keywords:* Header compression; Source modeling; Performance evaluation; Performance metrics

## 1. Introduction

Header compression improves the bandwidth efficiency over bandwidth scarce channels and is especially attractive in the presence of small packet payloads, which is often the case in practice. Interactive real-time

* Corresponding author. Tel.: +65 6796 8275; fax: +65 6775 9011.
*E-mail address:* cchiayua@dso.org.sg (C.Y. Cho).

1389-1286/$ - see front matter 
doi:10.1016/j.comnet.2005.09.036

**Nomenclature**

| | |
|---|---|
| $A$ | Channel A packet error process |
| $B$ | Channel B packet error process |
| $b$ | bit parameter of (W)LSB code |
| $\mathrm{BER_g}$ | bit error rate on condition that the channel state is good |
| $\mathrm{BER_b}$ | bit error rate on condition that the channel state is bad |
| $C$ | compressor process |
| $\overline{C}_j$ | mean compression success probability for the $j$th code in the codebook |
| CE | compression efficiency |
| CT | compression transparency |
| $D$ | decompressor process |
| $f$ | a generic flow of packets |
| $f_o$ | glow of observation |
| $g$ | number of complicated CHANGING fields in the header |
| $h_f$ | state truncation threshold; number of states in flow $f$ of truncated model |
| $K$ | number of codes in the codebook $\Psi$ |
| $m$ | length of the field in bits |
| $n_A$ | number of packets transmitted by the source $S$ to the compressor $C$ |
| $n_B$ | number of packets received by the compressor $C$ from the source $S$ |
| $o_{f_{(f',j')}}$ | offset parameter of (W)LSB code |
| $q_{(f,j)}$ | source model state transition probability, from state $(f,j)$ to $(f',j')$ |
| $r$ | context refresh period |
| $S$ | source process |
| $U_j$ | probability of using the $j$th code in the codebook |
| $w$ | size of context window; measure of robustness |
| $X$ | channel state process |
| $Y$ | bit error process |
| $Z$ | packet error process |
| $\beta_j$ | position of the first bit of the $j$th packet in a series of packets |
| $\Delta$ | source delta process |
| $\varepsilon$ | error due to truncation in Markov model |
| $\gamma_n$ | $n$th order probability distribution |
| $\eta$ | overhead incurred in 'discriminator bits' to signal code used in codebook |
| $\lambda_j$ | length of the $j$th packet |
| $\zeta$ | set of $(w,r)$ pairs satisfying the desired compression transparency criterion |
| $\Psi^K$ | codebook of $K-1$ (W)LSB codes with 1 fallback uncompressed code |

applications like IP telephony, multi-player network gaming and online chats all generate disproportionately small payloads in comparison to headers. In addition, non-real-time applications like web browsing predominantly carry payloads no more than a few hundred bytes.

The adoption of early header compression schemes over wireless links failed because early schemes like Van Jacobson Header Compression (VJHC) [1] were designed to operate over reliable wired links. Each loss of a compressed packet caused the compressor–decompressor context synchronization to be lost, generating a series of packets discards due to corrupted packets from decompression failures. The error condition persisted till packet retransmission initiated by higher layers (e.g. TCP) restored context synchronization. Over wireless links where high error rates and long round trip times are common, this caused header compression performance to deteriorate unacceptably. To deal with this, a number of schemes like IP Header Compression (IPHC) [10] and TCP-Aware Robust Header Compression (TAROC) [9] were proposed to offer robustness against packet loss in wireless channels. The ROHC is currently the state-of-the-art header compression

technique. A robust and extensible scheme, the ROHC is being developed by the IETF [2], and is an integral part of the 3rd Generation Partnership Project-Universal Mobile Telephone System (3GPP-UMTS) specification [3].

The deployment scenarios for header compression have been increasing over the years. Early header compression schemes like VJHC were first used over wired serial IP lines [1]. Current efforts mainly focus on developing header compression over 'last hop' wireless links and cellular links like UMTS [2]. Some of the most recent proposals explore header compression over multiple hops in a mobile ad hoc network [6], and even for high-speed backbone networks [14].

With the expected deployment of ROHC in increasingly diverse types of networks, the evaluation of Robust Header Compression performance in different scenarios becomes crucial. A number of tools and studies related to header compression performance can be found in the literature. The effect of ROHC on the subjective and objective quality of video was evaluated in [12] from a test-bed. Other studies evaluate header compression performance by simulation. Specialized ROHC simulators like the Acticom ROHC Performance Evaluation Tool [8], the Effnet HC-Sim [7] and the ROHC simulator-visualizer [13] have been developed for this purpose, though they are not readily available in public domain. Most studies in literature focus on various issues in header compression. An early study investigated the effect of inter-leaving at the packet source on RTP header compression [11]. A proposal on header compression over Multi-Protocol Layer Switching (MPLS) in high-speed networks investigated the tradeoff between compression gains and implementation cost [19]. The cost and performance due to the context establishment has been studied using an analytical model in [16] and the handover aspect was analyzed in [17]. The ROHC-TCP context replication mechanism was studied using packet traces in [15]. The notion of adaptive header compression was introduced in [18], where it was suggested that scheme parameters like the context window size and packet refresh rate be made adaptive to link conditions and packet sizes. However, the issue of how these parameters can be made adaptive was not addressed in the same paper.

While progress in several key aspects has been made in the above studies, we note that the above studies on header compression performance typically assume some particular network deployment scenario, i.e. over 'last-hop' wireless links. Moreover, we find that with the exception of few studies [7,11,15], the operating environment influencing the content and sequence of headers arriving at the compressor has not adequately addressed. The common setup used involves two nodes—the compressor and decompressor, separated by a wireless channel (simulated or real) in between. Indeed, this is a setup used in ROHC interoperability tests [8,12]. In most studies, the performance is evaluated by generating packets at the compressor (sometimes with real application payloads) for performing header compression. We note that the header contents generated in experimental conditions may be different from those in real operating environments. Because most studies do not ensure their headers are generated based on real-world behavior, they inadvertently assume idealized operating environments (e.g. handling non-concurrent flows) at the source. Moreover, the effect of packet loss between the source and compressor has not been studied in any existing work. Due to these shortcomings, packet headers produced under experimental conditions may become easily compressed at high efficiencies. Because this seems easily achieved, the interaction and tradeoffs between ROHC performance metrics like robustness and compression efficiency are often not examined in existing work.

The second issue deals with the design methodology of header compression schemes. Since the proposal of the first TCP/IP header compression scheme, VJHC [1] in 1990, it has been more or less a tradition for scheme design to be based on rules-of-thumb and qualitative descriptions of source headers [2,4]. Without a formal approach, the effects of different source and deployment scenarios cannot be precisely described, and optimization is difficult. As such, the notion of optimized schemes does not exist.

To deal with these issues, our first contribution in this paper is to propose a framework for modeling Robust Header Compression. The framework has five stochastic processes as its main components: the source, the source-compressor channel, the compressor, the compressor–decompressor channel, and finally the decompressor. By including the source process and source-compressor channel in the framework, a more complete picture of the main components affecting the performance is obtained. The framework is designed to be flexible enough to allow different scenarios to be modeled. For example, different deployment scenarios can be modeled by tuning the parameters of the channel models.

The ROHC has qualitatively defined three metrics for ascertaining the performance of an ROHC scheme: compression efficiency, robustness and compression transparency. We show that our modeling framework offers new perspectives to the definition and understanding of header compression performance metrics, using which we present a novel way to study the tradeoff dependencies between performance metrics.

Moving on from qualitative descriptions of header behavior to mathematical models, we present a real-world source model for studying header compression. This is the first time a source model is used for studying header compression. Built on a Markov model of the packet source, our source model captures the real-world behavior of the IP Identification header field in TCP flows. The effect of multiple concurrent flows on field behavior is modeled using a chain of Markov states for each packet flow. Using real traffic, we have built a real-world IPID source model for the average source. Interestingly, the source model may have wider applications because it also models the way packets are generated from a source with multiple concurrent flows. We also obtain the models for a busy source and the non-concurrent source in idealized operating environment. By plugging the desired source model into our modeling framework, the effect of different source scenarios on the performance outcome is investigated. Our results in Section 5 verify our intuition that the idealized operating environment of non-concurrency coupled with a perfect source-compressor channel leads to unrealistically high compression efficiencies almost independent of the robustness configuration.

Using our framework, we formally introduce the notion of optimized schemes. Presenting a tradeoff optimization procedure, we show, for the first time, that the parameters of a ROHC scheme can be tradeoff optimized based on the desired level of performance. This opens up the possibility of adaptively optimizing the entire set of parameters in a ROHC scheme, instead of adapting two parameters as suggested in [18] without optimization.

This paper is organized in the following structure. In the next section, we present the background and problem definition. Our framework for modeling header compression will be developed in Section 3. In Section 4, we present the source model for studying header compression. This is followed by our results from the performance and tradeoff study in Section 5. After a short discussion on future work, we end this paper with the significance of our contributions in conclusion.

The notation adopted in this paper is as follows: random variables are in upper case whilst values are in lower case. Vectors are assumed to be row vectors, and both vectors and matrices are denoted in bold, while the former is in lower case and the latter is in upper case. $(\cdot)^{\mathrm{T}}$ is used to denote the transpose of a matrix or vector.

## 2. Background and problem definition

We begin by giving an overview of the ROHC system. After presenting the background on encoding methods and robustness, we then proceed to define the objective of ROHC scheme design. At the end of this section, we introduce a channel model which will be used in later sections.

### 2.1. Overview of Robust Header Compression

Fig. 1 gives a pictorial overview of the ROHC system over a wireless channel. In general, a number of packet flows pass through the system simultaneously. The compressor compresses each packet by referring to previous headers of the same flow. This is done by maintaining a window of $w$ contexts per flow, where each $n_f$th context stores the $n_f$th previous header. As will be elaborated upon, the window of $w$ contexts are required for robustness. The decompressor is only required to maintain a single context per flow. This context stores the latest header which has been verified to be successfully decompressed through passing the Cyclic Redundancy Check (CRC). The decompressor may then feedback the compressor upon verification success or failure. To facilitate feedbacks, each packet is uniquely identified with a Sequence Number. In ROHC-TCP, this is called the Master Sequence Number (MSN), which is maintained as a flow-specific counter [5].

The actions performed by the compressor and decompressor are state-dependent, controlled by the compressor and decompressor state-machines respectively. Three compressor states are defined in the ROHC framework: Initialization and Refresh (IR) state, First Order (FO) state and Second Order (SO) state [2]; the three states are reduced to two in ROHC-TCP: IR state and Compressed (CO) state, for which the latter

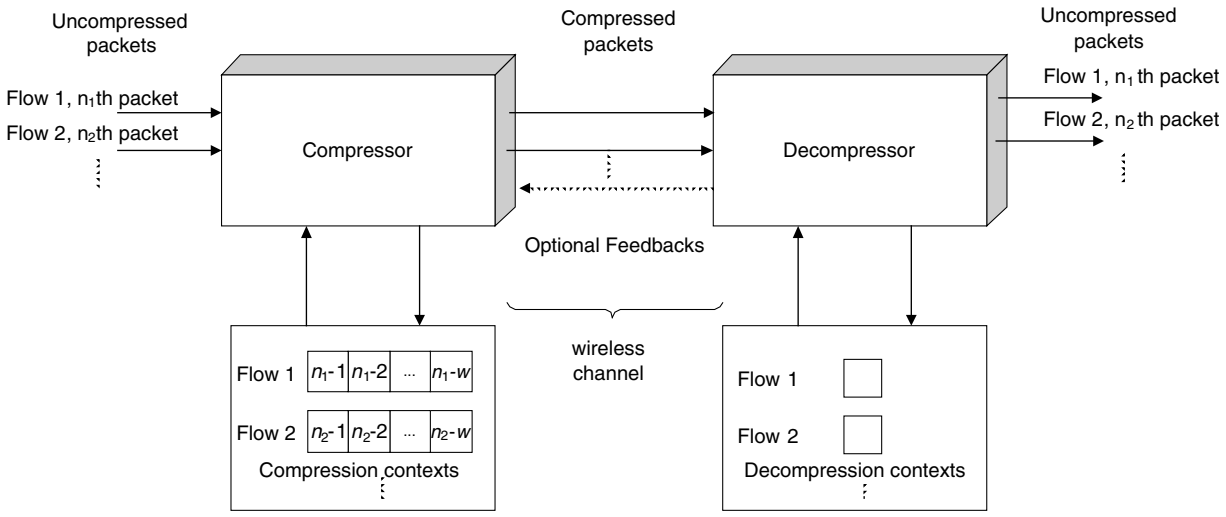


Fig. 1. Pictorial overview of Robust Header Compression system.

state is synonymous to the FO state [5]. The name of the state is indicative of the operation in that state: In IR state, the full header is sent uncompressed; In FO (SO) state, the first (second) order differences between packets are used to perform compression. Naturally, header compression is the most efficient in the SO state.

For the purpose of clarity, we will implicitly adopt the two-state compressor state machine used in ROHC-TCP for our problem definition and analysis. However, it is not too difficult to extend our analysis using the same approach for the three-state case.

### 2.2. Encoding methods and robustness

Header compression is possible due to the fact that most header fields either do not change throughout a flow, or increase with small deltas between consecutive packets of a flow. To deal with this, the IETF ROHC Working Group came up with the taxonomy for header fields. Based on the qualitative descriptions of header field behaviors, header fields are classified into three broad categories for different compression strategies: STATIC, INFERRED and CHANGING.

STATIC fields do not change and need only be communicated once per flow. Appropriately, this is called STATIC encoding. INFERRED fields, on the other hand, do not even need to be transmitted.

Most of the complexities required in header compression schemes are attributed to a relatively small number of CHANGING fields. Fields like IP Identification (IPID), TCP Sequence Number and Acknowledgment Number are known to mostly increase between headers with relatively small deltas. The type of encoding used for these deltas makes the difference between a good and poor scheme. In VJHC, CHANGING fields are encoded using the deltas of consecutive headers. This means that the encoded form of a field takes on a value equivalent to the delta from the reference field in the previous header. For example, if the TCP Sequence Numbers in two consecutive headers are 2900000 and 2900360, then the field in the second header can be encoded into its delta, 360 instead. To facilitate encoding (decoding), the previous packet header is stored in the context at the compressor (decompressor). Though this approach is simple, the decompression of each header requires the previous header to be received correctly. This approach is unsuitable over wireless links because a single packet loss invalidates the decompression context to be used for the next packet, and so the compressor–decompressor context synchronization is lost. Thus, the next packet will not decompress correctly and is discarded. By induction, all subsequent decompression contexts also become invalid, causing an avalanche of packet discards till higher layer (e.g. TCP) retransmission mechanisms are activated. This solution is unsatisfactory because higher layer recovery incurs long delay and high overhead. This phenomenon is known as damage propagation.

The Least Significant Bit encoding (LSB) is proposed in ROHC as an alternative to delta encoding. A LSB code is defined by two parameters, $(b, o_f)$. Instead of compressing fields into deltas, it requires the $b$ least significant bits of the field to be sent over the channel. A LSB encoded field can be decoded unambiguously if the *difference* of the original value with respect to the reference value is *within* the *interpretation interval* $[-o_f, 2^b - 1 - o_f]$. Using the previous example where we encode the value 2900360 using 2900000, suppose we first define a LSB code $(b, o_f) = (10, 0)$ known to both the compressor and decompressor. With knowledge of the previous value, 2900000, and receiving only the 10 least significant bits of 2900360, i.e. 0110001000 in binary, the decompressor simply locates the binary sequence in the range $[2900000, 2900000 + 2^{10} - 1]$ and thus is able to uniquely identify the next value as 2900360.

Note that the field can be encoded *only if* the delta is within the interval. Using the same example, if the LSB code $(4, 0)$ is used instead, then only values between 2900000 to 2900015 inclusive can be encoded without ambiguity. In this case, the LSB code defined by $(4, 0)$ has failed to encode the field and the compressor has to decide on other alternatives. Note that since the size of the interpretation interval is $2^b$, only $b$ bits are required to identify the position within the interval, and thus only $b$ bits are communicated in encoded form.

To cope with the case where a LSB code fails to encode a field, a series of LSB codes can be used as further attempts to LSB encode the field. If all specified LSB codes fail, the compressor falls back to sending the field uncompressed. The latter can be seen as the final 'code'. When the offset is constant, a set of $K - 1$ LSB codes and one uncompressed 'code' constitutes the codebook for a single field, and can be defined as $\Psi^K = \{\{(b_i, o_f)\}_{i=1}^{K-1}, m\}$, where $b_j > b_i$ if $j > i$, $m$ is the length of the field in bits, and $K \in [1, m + 1]$ is the size of the codebook. The compressor shares the same codebook with the decompressor, and the compressor signals the code used with up to $\lceil \log_2 K \rceil$ 'discriminator bits', which are incurred as overhead. In ROHC-TCP, the overhead may be less than $\lceil \log_2 K \rceil$ bits due to the use of Huffman coding, and this is usually necessary when $K$ is large.

Note that in our definition of a codebook, $\Psi^K$, we have assumed a constant offset parameter, $o_f$, for all the LSB codes in the codebook. By defining the interpretation interval as $[-o_f, 2^b - 1 - o_f]$, the ROHC allows the position of the interpretation interval (with respect to the reference field) to be shifted through the pre-defined offset $o_f$. Although there is no formal requirement to do so, the ROHC recommends defining $o_f$ based on field behavior [2], i.e. if the field value only increases, then $o_f$ should be $-1$. If the field value is non-decreasing, then $o_f$ should be 0. If it is strictly decreasing, then it should be $2^b$. For example, by simple substitution, the interpretation interval for the strictly decreasing case is $[-2^b, -1]$. Using 2900000 again as the reference value and this time with $(b, o_f) = (10, 2^{10})$ as the LSB code, only *values* within the range $[2900000 - 2^{10}, 2900000 - 1]$ can be encoded. It is thus evident that this offset value is best suited for a field with strictly decreasing behavior.

Note that LSB encoding alone does not provide any form of robustness because it still requires exact synchronization between the compressor and decompressor contexts. The robustness is due to an extension of it, the window-based LSB (WLSB), which does not require exact synchronization. In WLSB, the compressor keeps a *sliding window* of the *last w contexts* for each flow, but the decompressor maintains only the *last successfully decompressed context* (see Fig. 1) for each flow. Thus, the LSB is in fact a specific case of WLSB with $w = 1$. For each packet, *the compressor ensures that the compressed packet can be decompressed using any context within its sliding window*. Thus, the decompressor's context is valid as long as it is identical to *any one context* inside the sliding window used at the compressor. We can see that robustness is achieved: only one out of $w$ contexts at the compressor need to be synchronized with that at the decompressor and in the worst case, the scheme can tolerate up to $(w - 1)$ consecutive packet drops without damage propagation.

We now explain *how* "the compressor ensures the compressed packet can be decompressed using any context within its sliding window". Recall from our explanation on the LSB code $(b, o_f)$ that an encoded field can be decoded unambiguously if the *difference* of the original value with respect to the reference value is *within* the *interpretation interval* $[-o_f, 2^b - 1 - o_f]$. We now extend this reasoning to the WLSB code $(b, o_f)$ where there is a window of $w$ contexts (and thus a window of $w$ reference values). If the compressor wants to ensure that the encoded field can be decoded using any context within its sliding window, then it encodes the field *only if* this condition is satisfied: The *difference* of the original value with respect to *each* reference value in the window of contexts is *within* the *interpretation interval* $[-o_f, 2^b - 1 - o_f]$.

We use the same example where we tried to encode 2900360, this time with the *WLSB code* $(b, o_f) = (10, 0)$ of window size $w = 2$. Suppose the compressor has two previous values, 2899500 and 2900000, as references. Since $2900360 \in [2899500, 2899500 + 2^{10} - 1]$ and $2900360 \in [2900000, 2900000 + 2^{10} - 1]$, by receiving only the 10 least significant bits of 2900360, the decompressor can use *either reference value* to uniquely identify the next value as 2900360. However, with two conditions to be satisfied before the value can be encoded, a slightly larger value, e.g. 2900700, cannot be encoded using the same code, since $2900700 \notin [2899500, 2899500 + 2^{10} - 1]$.

WLSB achieves robustness by *preventing* damage propagation. The ROHC uses two other mechanisms for *fast recovery* from damage propagation: periodic context refreshes and optional feedbacks, instead of relying on higher layer recovery mechanisms. Periodic context refreshes simply means sending uncompressed packets at periodic intervals of $r$ packets. With this mechanism in place, damage propagation can no longer extend beyond $r$ packets easily. Feedbacks from the decompressor further accelerate recovery through explicit retransmission requests at the header compression layer. However, this is an optional feature and we assume the absence of feedbacks in this paper.

Finally, note that for a single field, we define the set of parameters denoting a Robust Header Compression scheme as $\{\Psi^K, w, r\}$, where $\Psi^K$ is the codebook such that $\Psi^K = \{\{(b_i, o_f)\}_{i=1}^{K-1}, m\}$. Extending this to include all CHANGING fields in the header, the entire set of parameters defining a Robust Header Compression scheme becomes $\{\Psi_1^{K_1}, \Psi_2^{K_2}, \ldots, \Psi_g^{K_g}, w, r\}$ where $g$ is the number of complicated CHANGING fields.

At this stage, the objective of scheme design is to determine *suitable values* for these parameters given *external conditions* over which the designer has no control of. We will see that our modeling framework enables a more formal and meaningful definition of the objective of scheme design.

### 2.3. Channel model

We are interested in a model for the packet loss/survival process over a channel. A variety of models attempting to model the packet loss/survival process exists in the literature. We select a particular model which has been found to be relatively accurate [20], and which can be easily adjusted to model wireless channels in high and low speed mobility [21]. We outline an adapted version of this model and the interested reader is referred to [20] for details.

Let $\{Z(j): j = 1, 2, \ldots\}$ be the packet loss/survival stochastic process over the channel, with event space $\{1, 0\}$ denoting the events of packet survival and packet corruption respectively. $\{Z(j)\}$ can be defined from the lower-level bit error/error-free process.

The bit error/error-free process is modeled by the well-known Gilbert–Elliot model. Let $X(i) \in \{\text{good}, \text{bad}\}$ denote the channel state during the transmission of bit $i$. The channel state process $\{X(i): i = 1, 2, \ldots\}$ is modeled by a two-state Markov chain as shown in Fig. 2. In each state, a state-dependent bit error rate exists in the duration of that bit transmission, denoted by $\text{BER}_\text{g}$ and $\text{BER}_\text{b}$, where $\text{BER}_\text{g} < \text{BER}_\text{b}$. The effects of Forward Error Correction (FEC) can be taken into consideration when defining the bit error rates. Practical values of state transition probabilities and state-dependent bit error rates due to different mobility speeds have been found in [21] and will be used in this paper.

Let $\{Y(i): i = 1, 2, \ldots\}$ be the bit error/error-free process with event space $\{1, 0\}$ denoting the events of bit error-free and bit error respectively. Then the outcome of bit $i$ conditioned on the channel state is given by

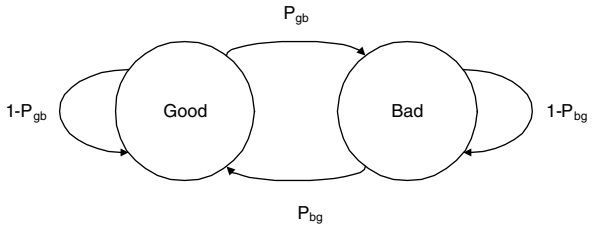


Fig. 2. Markov model of channel state process.

$$\begin{aligned} &P(Y(i)=0|X(i)=\text{good})=\text{BER}_\text{g},\\ &P(Y(i)=0|X(i)=\text{bad})=\text{BER}_\text{b},\\ &P(Y(i)=1|X(i)=\text{good})=1-\text{BER}_\text{g},\\ &P(Y(i)=1|X(i)=\text{bad})=1-\text{BER}_\text{b}. \end{aligned} \tag{1}$$

Let the $j$th packet start at bit $\beta_j$ and end at bit $\beta_j+\lambda_j-1$. The packet remains uncorrupted when all bits in the range $[\beta_j,\beta_j+1,\ldots,\beta_j+\lambda_j-1]$ are error-free. Therefore, at each $j$, the packet loss probability of $Z(j)$ can be defined as

$$P(Z(j)=1)=P\left(\bigcap_{i=\beta_j}^{\beta_j+\lambda_j-1} Y(i)=1\right). \tag{2}$$

As a result of the above expression, the *error-free* probability of the $j$th packet given its initial channel state $X(\beta_j)=x_{\beta_j}$ can be evaluated as

$$P(Z(j)=1|X(\beta_j)=x_{\beta_j})\equiv P^{1|x_{\beta_j}}_{Z_j|X_{\beta_j}}=\boldsymbol{x}_j\boldsymbol{M}^{\lambda_j-1}\boldsymbol{e}^{\mathrm{T}},$$

where

$$\begin{aligned} &\boldsymbol{x}_j=\begin{cases}[\,1 \quad 0\,], & x_{\beta_j}=\text{good},\\ [\,0 \quad 1\,], & x_{\beta_j}=\text{bad},\end{cases}\\ &\boldsymbol{M}=\begin{bmatrix}p_{gg}(1-\text{BER}_\text{g}) & p_{gb}(1-\text{BER}_\text{g})\\ p_{bg}(1-\text{BER}_\text{b}) & p_{bb}(1-\text{BER}_\text{b})\end{bmatrix},\\ &\boldsymbol{e}=[\,(1-\text{BER}_\text{g}) \quad (1-\text{BER}_\text{b})\,], \end{aligned} \tag{3}$$

and $P(Z(j)=1|X(\beta_j)=x_{\beta_j})\equiv P^{1|x_{\beta_j}}_{Z_j|X_{\beta_j}}$ is defined for compactness. For analyzing a group of consecutive packets, a useful auxiliary result is the probability that the $j$th packet is error-free *and* the $(j+1)$th packet starts at a particular channel state, *given* the initial channel state at the start of the $j$th packet:

$$P(Z(j)=1,X(\beta_{j+1})=x_{\beta_{j+1}}|X(\beta_j)=x_{\beta_j})\equiv P^{1,x_{\beta_{j+1}}|x_{\beta_j}}_{Z_j,X_{\beta_{j+1}}|X_{\beta_j}}=\boldsymbol{x}_j\boldsymbol{M}^{\lambda_j-1}(\boldsymbol{e}')^{\mathrm{T}},$$

where

$$\boldsymbol{e}'=\begin{cases}[\,p_{gg}(1-\text{BER}_\text{g}) \quad p_{bg}(1-\text{BER}_\text{b})\,], & x_{\beta_{j+1}}=\text{good},\\ [\,p_{gb}(1-\text{BER}_\text{g}) \quad p_{bb}(1-\text{BER}_\text{b})\,], & x_{\beta_{j+1}}=\text{bad}.\end{cases} \tag{4}$$

Finally, it is not too difficult to derive similar expressions for variations of other packet *error* probabilities given the initial channel state

$$\begin{aligned} &P^{0|x_{\beta_j}}_{Z_j|X_{\beta_j}}=1-P^{1|x_{\beta_j}}_{Z_j|X_{\beta_j}},\\ &P^{0,x_{\beta_{j+1}}|x_{\beta_j}}_{Z_j,X_{\beta_{j+1}}|X_{\beta_j}}=P^{x_{\beta_{j+1}}|x_{\beta_j}}_{X_{\beta_{j+1}}|X_{\beta_j}}-P^{1,x_{\beta_{j+1}}|x_{\beta_j}}_{Z_j,X_{\beta_{j+1}}|X_{\beta_j}}. \end{aligned} \tag{5}$$

## 3. A framework for modeling header compression

We begin this section with a high-level presentation of our modeling framework in terms of five stochastic processes—a source process, two channel processes, a compression process and a decompression process. We give the initial broad definition for the source process, and describe the channel processes based on existing channel models. We then show how the compression and decompression processes can be defined based on the source process and channel processes. Extending current definitions, we offer new perspectives to the three performance metrics. We end this section by showing how the framework can be used to model different source and deployment scenarios.

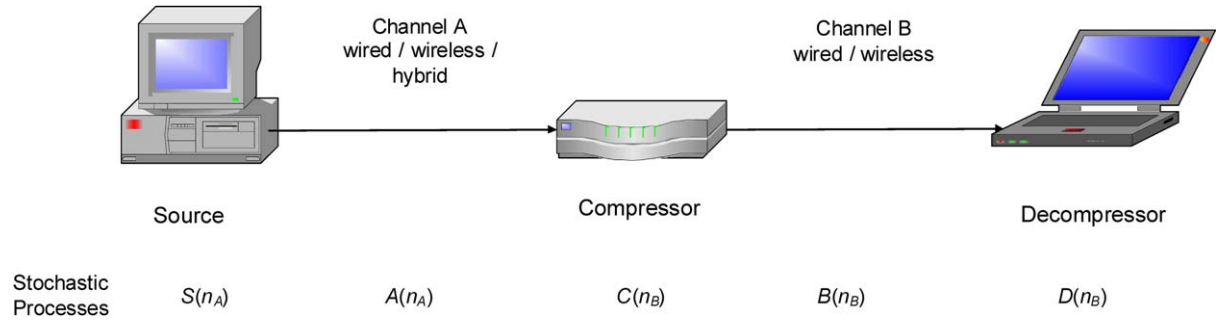


Fig. 3. Header compression deployment in a general network scenario.

### 3.1. Overview of modeling framework

Fig. 3 shows header compression deployment in a general scenario. The source node is the generator of packet headers, transmitting packets to the remote compressor through Channel A. The compressor compresses the packet headers and transmits compressed packets through Channel B to the decompressor. The passage beyond the decompressor has no effect on the header compression system. As illustrated in Fig. 3, this can be modeled with five stochastic processes. Trivial and starkly simple, we will show that this representation allows different source and deployment scenarios to be modeled.

### 3.2. The source process

Different protocol fields possess different and often independent behavior, making it difficult to have a single source model describing all the fields in the entire header. As a start, with the assumption of independence, the approach is to develop source models for each field individually. To analyze different fields, we simply use different source models.

For each field, the source of the flow under observation, $f_o$, is a discrete-time stochastic process, $\{S_{f_o}(n_A)\colon n_A = 0, 1, \ldots\}$, which takes values in the discrete space $[0, 2^m - 1]$ for a field of $m$ bits long. A convenient way of simplifying the process $\{S_{f_o}(n_A)\}$ is to view it as having an initial value $s_{f_o}(0)$ and being generated from a 'delta process', $\{\Delta_{f_o}(n_A)\colon n_A = 0, 1, \ldots\}$, such that

$$\begin{aligned} \Delta_{f_o}(n_A) &= S_{f_o}(n_A) - S_{f_o}(n_A - 1), \\ \delta_{f_o}(n_A) &= s_{f_o}(n_A) - s_{f_o}(n_A - 1). \end{aligned} \tag{6}$$

Thus, in general, the source of a flow of observation can be modeled by its delta process $\{\Delta_{f_o}(n_A)\}$ and an initial value $s_{f_o}(0)$. Conversely, we can express the difference between $s_{f_o}(n_A)$ and $s_{f_o}(n_A - h)$ in terms of deltas

$$s_{f_o}(n_A) - s_{f_o}(n_A - h) = \sum_{i=n_A-h+1}^{n_A} s_{f_o}(i) - s_{f_o}(i-1) = \sum_{i=n_A-h+1}^{n_A} \delta_{f_o}(i). \tag{7}$$

Note that during header compression operation, the compressor transmits a number of least significant bits defined by $b_i$ due to its choice of code $(b_i, o_f)$ in its codebook $\Psi^K$. The above delta process is a means to model the source process, and so should not be confused as the output of the compressor.

Let us apply the concept of source and delta processes to the IPID field. The IPID is a unique identifier for packets from a source. A predominant implementation is to use a common counter shared by all flows, incremented for every packet sent from the source. For a single flow, consecutive packets carry values with small sequential offsets. This is known to account for the small IPID deltas characterization in literature [4]. As an example, consider a source transmitting 2 flows (flows 1 and 2) concurrently. Fig. 4 illustrates the sequence of values observed when either flow is chosen to be the flow of observation.

For the rest of this paper, the notion of the chosen flow of observation is assumed to apply for the source process, and the flow subscript $f_o$ will be dropped from $S_{f_o}(n_A)$ and $\Delta_{f_o}(n_A)$.

| | | | | | | | | | | |
|---|---|---|---|---|---|---|---|---|---|---|
| IPID value: | | 1 | 2 | 3 | 4 | 5 | 6 | 7 | 8 | 9 | 10 |
| Flow ID: | | 1 | 2 | 2 | 1 | 1 | 1 | 2 | 1 | 2 | 1 |
| $f_o$=1 | $s_1(n_A)$: | 1 | - | - | 4 | 5 | 6 | - | 8 | - | 10 |
| | $\delta_1(n_A)$: | - | - | - | +3 | +1 | +1 | - | +2 | - | +2 |
| $f_o$=2 | $s_2(n_A)$: | - | 2 | 3 | - | - | - | 7 | - | 9 | - |
| | $\delta_2(n_A)$: | - | - | +1 | - | - | - | +4 | - | +2 | - |

Fig. 4. Observed sequences for different flows of observations.

### 3.3. The channel processes

Let Channel A be the channel between the source and compressor. To model the packet loss in the passage through Channel A, we define a packet survival/loss discrete-time stochastic process $\{A(n_A)\colon n_A = 1,2,\ldots\}$, such that

$$A(n_A) = \begin{cases} 1, & n_A\text{th packet is not corrupted in Channel A} \\ 0, & n_A\text{th packet is corrupted in Channel A.} \end{cases} \tag{8}$$

Existing channel models like that presented in Section 2.3 can be used to model this process. We also derive another stochastic process from $\{A(n_A)\}$, called the Channel A *loss run process*, $\{L_A(j_A)\colon j_A = 1,2,\ldots\}$, where for a particular index $j_A$, the number of packets lost between two nearest loss-free packets is a random variable $L_A(j_A)$. For example, in the following sample sequence of $\{A(n_A)\}$: $1,1,0,1,1,1,1,0,0,1,0,0,0,1,\ldots$, the sequence of loss run lengths would be: $0,1,0,0,0,2,3,\ldots$ The probability of a loss run, $P(L_A(j_A) = l_A)$, can be expressed as

$$P(L_A(j_A) = l_A) = P(A(n_A - 1) = 0, \quad A(n_A - 2) = 0, \ldots, \quad A(n_A - l_A) = 0, \quad A(n_A - l_A - 1) = 1 | A(n_A) = 1), \tag{9}$$

where the $j_A$th run is defined in terms of the Channel A process as $j_A = (\sum_{i=1}^{n_A} a(i)) - 1$.

Let Channel B be the channel between the compressor and decompressor. In the same way

$$B(n_B) = \begin{cases} 1, & n_B\text{th packet is not corrupted in Channel B} \\ 0, & n_B\text{th packet is corrupted in Channel B,} \end{cases} \tag{10}$$

where $n_B = (\sum_{i=1}^{n_A} a(i))$ is the number of packets from the source successfully received by the compressor and

$$P(L_B(j_B) = l_B) = P(B(n_B - 1) = 0, \quad B(n_B - 2) = 0, \ldots, \quad B(n_B - l_B) = 0, \quad B(n_B - l_B - 1) = 1 | B(n_B) = 1), \tag{11}$$

where the $j_B$th run in Channel $B$ is defined by $j_B = (\sum_{i=1}^{n_B} b(i)) - 1$.

Note that the stochastic process $\{B(n_B)\colon n_B = 1,2,\ldots\}$ maintains a separate counter $n_B$ due to the fact that $B(n_B)$ is defined only in the event $A(n_A) = 1$. We make the assumption that $\{A(n_A)\}$ and $\{B(n_B)\}$ are independent, which is reasonable in practice. Then $\{B(n_B)\}$ is another channel process independently defined from the packet loss/survival model in Section 2.3.

As $n_A \to \infty$, it is well-known that the Gilbert–Elliot channel state model converges to a steady-state distribution:

$$\begin{aligned} P_X^g &\equiv P(X(n_A) = g)|_{n_A \to \infty} = \frac{P_{bg}}{P_{gb} + P_{bg}}, \\ P_X^b &\equiv P(X(n_A) = b)|_{n_A \to \infty} = 1 - P_X^g. \end{aligned} \tag{12}$$

This allows the steady-state probability of the packet loss process and loss run process to be formulated. Focusing on Channel $A$ with results equally applicable to Channel $B$, we know from Eq. (9) as $n_A \to \infty$, $j_A \to \infty$ that

$$P(L_A = l_A) = \frac{P(A_0 = 1, A_{-1} = 0, \ldots, A_{-l_A} = 0, A_{-l_A - 1} = 1)}{P(A_0 = 1)}, \tag{13}$$

where $A_{-l} \equiv A(n_A - l)|_{n_A \to \infty}$. We assume that all packets passing through Channel A are of the same length, so that we need not be concerned with differences in packet lengths at steady state. The denominator in Eq. (13) is the probability of packet survival in Channel A. Using results in Section 2.3, the steady-state probability of the packet loss process can be evaluated as

$$P(A_0 = 1) = P_{A|X}^{1|g} P_X^g + P_{A|X}^{1|b} P_X^b. \tag{14}$$

The numerator in Eq. (13) can be derived by considering, for each packet, the probability for all combinations between (i) the initial channel state of the current packet, (ii) the current packet loss/survival, and (iii) the channel state after the current packet. These combinations were introduced in Eqs. (3–5), and the result can be expressed in matrix form as

$$P(A_0 = 1, A_{-1} = 0, \ldots, A_{-l_A} = 0, A_{-l_A-1} = 1) = [P_X^g \quad P_X^b] \begin{bmatrix} P_{A,X|X_{-1}}^{1,g|g} & P_{A,X|X_{-1}}^{1,b|g} \\ P_{A,X|X_{-1}}^{1,g|b} & P_{A,X|X_{-1}}^{1,b|b} \end{bmatrix} \begin{bmatrix} P_{A,X|X_{-1}}^{0,g|g} & P_{A,X|X_{-1}}^{0,b|g} \\ P_{A,X|X_{-1}}^{0,g|b} & P_{A,X|X_{-1}}^{0,b|b} \end{bmatrix}^{l_A} \begin{bmatrix} P_{A|X}^{1|g} \\ P_{A|X}^{1|b} \end{bmatrix}. \tag{15}$$

We will verify our steady-state analysis by comparison with simulation results in the results section.

### 3.4. The compressor processes

Similar to $\{B(n_B)\}$, the compressor process $\{C(n_B)\colon n_B = 1, 2, \ldots\}$ is defined only in the events $\{A(n_A) = 1 \forall n_A = 1, 2, \ldots\}$. We have found it convenient to represent the compressor process with the following event space:

$$C(n_B) = \begin{cases} 1, & s(n_A) \text{ can be compressed,} \\ 0, & s(n_A) \text{ cannot be compressed.} \end{cases} \tag{16}$$

Recall from Section 2.2 that the set of parameters defining a ROHC scheme for a single field under study is $\{\Psi^K, w, r\}$ where $\Psi^K = \{\{(b_i, o_f)\}_{i=1}^{K-1}, m\}$. The objective is to define the compressor process $C(n_B)$ given $\{\Psi^K, w, r\}$.

The compressibility of a field depends on a number of issues: (i) the size of the context window, $w$, (ii) the parameters in the codebook $\Psi^K$, (iii) presence of packet losses in Channel A, and (iv) the use of intermediate encoding.

To focus on the effect of context window size, we first make the assumption of a perfect Channel A and deal with the case of the simplest codebook ($K = 2$) without any complicating intermediate encoding. The effect of the context window size on the compressibility of a field can be seen from the requirements of robustness in Section 2.2. Note in particular that the compressor encodes the field *only if* this condition is satisfied: The *difference* of the original value with respect to *each* reference value in the window of contexts is *within* the *interpretation interval* $[-o_f, 2^b - 1 - o_f]$. Given that the compressor is using a single fixed WLSB code $(b, o_f)$ and denoting the interpretation interval $[-o_f, 2^b - 1 - o_f]$ as $V(o_f, b)$, the event of compression success occurs when the difference between $s(n_A)$ and *each* $h$th previous context lies within the interpretation interval

$$\begin{aligned} &(s(n_A) - s(n_A - h)) \in V(o_f, b), \quad \forall h = 1, 2, \ldots, w \\ &\therefore \left( \sum_{i=n_A-h+1}^{n_A} \delta(i) \right) \in V(o_f, b), \quad \forall h = 1, 2, \ldots, w. \end{aligned} \tag{17}$$

In practice, header fields increase monotonically in the duration of a flow except when the occasional wrap-around occurs. This means that the largest difference between $s(n_A)$ and any $s(n_A - h)$, $h = 1, 2, \ldots, w$ is given by $s(n_A) - s(n_A - w)$. Thus, the compression success probability can be evaluated as

$$P(C(n_B) = 1 | o_f, b, w) = P\left( \sum_{i=n_A-w+1}^{n_A} \Delta(i) \in V(o_f, b) \right). \tag{18}$$

Note that the compression success probability is not conditioned on $r$ though it is part of the set of parameters $\{\Psi^K, w, r\}$ in the scheme because it has no effect on the compressibility of a field. However, $r$ determines the scheduling of uncompressed packets. This is to be conditioned in the decompression process.

The significance of Eq. (18) is that the probability of compression success depends on up to the $(w-1)$th order probabilities of the source delta process. As we will later demonstrate, Eq. (18) can be used for studying and verifying the high-order probabilities of a source model. Also, Eq. (18) requires a source model to remain reasonably accurate at high orders.

We now discuss the effect of the issue (ii): the parameters in the codebook $\Psi^K$. This can be done by extending the above case of a single code to the codebook of $K$ codes: $\Psi^K = \{\{(b_i, o_f)\}_{i=1}^{K-1}, m\}$ where $K = 2$. Due to the presence of $K$-1 WLSB codes in the codebook, a given field value is considered compressible if *at least one* of the $K-1$ codes encodes the field successfully, i.e. the event of compression success using the codebook $\Psi^K$ is the *union* of compression success events for each WLSB code in the codebook $\Psi^K = \{\{(b_i, o_f)\}_{i=1}^{K-1}, m\}$ with the following result:

**Proposition 1.** *Given the WLSB codebook* $\Psi^K = \{\{(b_i, o_f)\}_{i=1}^{K-1}, m\}$ *in the set of parameters* $\{\Psi^K, w, r\}$ *in the scheme, where* $b_j > b_i$ *if* $j > i$, *the compression success probability of the codebook is the same as that of the* $(K-1)$*th WLSB code* $(b_{K-1}, o_f)$, *i.e.* $P(C(n_B) = 1|\Psi^K, w) = P(C(n_B) = 1|o_f, b_{K-1}, w)$.

**Proof.** The event $C(n_B) = 1$ occurs when *any* of the $K-1$ WLSB codes in the codebook encodes $s(n_A)$ successfully, i.e.

$$P(C(n_B) = 1|\Psi^K, w) = P\left(\bigcup_{i=1}^{K-1} C(n_B) = 1|o_f, b_i, w\right).$$

From Eq. (18), we know that the compression success probability of a WLSB code $(b, o_f)$ depends on the size of its interpretation interval and we can modify the above expression as

$$P(C(n_B) = 1|\Psi^K, w) = P\left(\sum_{i=n_A-w+1}^{n_A} \Delta(i) \in \bigcup_{i=1}^{K-1} V(o_f, b_i)\right).$$

Due to the property that $b_i < b_j$ if $i < j$, and recalling that $V(o_f, b) \triangleq [-o_f, 2^b - 1 - o_f]$, then it is straightforward to see that $V(o_f, b_i) \subset V(o_f, b_j)$ if $i < j$. It follows by induction that that $V(o_f, b_i) \subset V(o_f, b_{K-1}) \forall i \in \mathbb{Z}^+$ and $i < K-1$. Therefore, the probability of compression success of the codebook is the same as that of the last WLSB code $(b_{K-1}, o_f)$. □

Note that Proposition 1 makes no assumptions on Channel A and its result is equally applicable to non-ideal Channel A conditions. We now consider the effect of packet losses in Channel A by illustration. Suppose for $w = 3$, we have the following sequence of values: $\ldots, s(n_A - 7), \cancel{s(n_A - 6)}, \cancel{s(n_A - 5)}, s(n_A - 4), \cancel{s(n_A - 3)}, s(n_A - 2), \cancel{s(n_A - 1)}, s(n_A), \ldots$, where the current value, $s(n_A)$, is to be compressed and values marked with double strike through were corrupted in Channel A. We find that Eq. (18) is no longer correct since the $w$th previous value is $s(n_A - 7)$ instead of $s(n_A - 3)$. The number of packets lost between two correctly received packets in the above example is given by values from the loss run process, i.e. $L_A(j_A - 2) = 2$, $L_A(j_A - 1) = 1$ and $L_A(j_A) = 1$.

If we define $l_{AT}$ as the total number of packets lost *since the wth previous context*, then the following result is evident from the above example:

$$P(C(n_B) = 1|\Psi^K, w) = \sum_{l_{AT}=0}^{n_B-n_A} P\left(\sum_{i=n_A-l_{AT}-w+1}^{n_A} \Delta(i) \in V(o_f, b_{K-1})\right) \times P\left(\left(\sum_{i'=j_A-w+1}^{j_A} L_A(i')\right) = l_{AT}\right). \quad (19)$$

Note that the difference $(n_B - n_A)$ is used in Eq. (19) because for some particular $n_A$ and $n_B$, $(n_B - n_A)$ is the total number of packets lost in Channel A.

Eq. (19) can be used readily if the compressor attempts to use the codebook $\Psi^K$ on the field directly. In ROHC specifications, it is common to find some fields being processed with intermediate encoding before using the WLSB codebook to encode the field into its final compressed form [5]. The motivation for using

intermediate encoding is to obtain better gains. Though intuitive, this is yet unproven in open literature. Here, we show how intermediate encoding on the IP Identification (IPID) field can be studied through some simple modification in our compressor process.

The Master Sequence Number (MSN) is an ROHC field which increments for every ROHC packet transmitted to the decompressor within a flow (see Section 2.1). We will see that this characteristic is similar to the IPID field. As intermediate encoding it is specified that the MSN field be subtracted from the IPID field (this is in fact performed using an encoding method called 'INFERRED-OFFSET') [5]. Due to this intermediate step, the modified input to the WLSB codebook at the compressor becomes $s'(n_A) = s(n_A) - msn(n_A)$. The result of this is that

$$s'(n_A) - s'(n_A - (l_{AT} + w)) = [s(n_A) - s(n_A - (l_{AT} + w))] - w \text{ or } \sum_{i=n_A - l_{AT} - w + 1}^{n_A} \delta'(i) = \left( \sum_{i=n_A - l_{AT} - w + 1}^{n_A} \delta(i) \right) - w. \tag{20}$$

Note that we have used the result $msn(n_A) - msn(n_A - (l_{AT} + w)) = w$ to obtain the above expression. Recall from Section 2.1 that the MSN is an ROHC field *added at the compressor*, and that $l_{AT}$ is the total number of packets lost in Channel A since the $w$th previous context. Then due to the fact that the MSN field increments for each packet of the same flow received (and transmitted) by the compressor, we yield the above expression.

### 3.5. The decompressor process

The decompressor process $\{D(n_B): n_B = 1, 2, \ldots\}$ is defined only in the events $\{A(n_A) = 1 \ \forall n_A = 1, 2, \ldots\}$. We define it as a discrete-time stochastic process with the following event space:

$$D(n_B) = \begin{cases} 1, & s(n_A) \text{ is decompressed successfully,} \\ 0, & s(n_A) \text{ is not decompressed successfully.} \end{cases} \tag{21}$$

Note that decompression failure arises when a packet fails its CRC integrity check. The reason for this can be attributed to channel errors (corruptions), and/or when the decompression context is invalid. In either case, the packet decodes erroneously. Thus, failure occurs once a packet is corrupted in Channel B, i.e. $D(n_B) = 0$ if $B(n_B) = 0$, but not the converse.

Two key factors determine whether $s(n_A)$ can be decompressed: (i) whether it has been compressed, and if so, (ii) the number of packets between the current packet and the last successfully decompressed packet.

We first consider the effect of whether $s(n_A)$ has been compressed. In the event that $s(n_A)$ was uncompressed, then decompression fails *only if* the packet was corrupted in Channel B. $s(n_A)$ can be uncompressed if $C(n_B) = 0$, or if the compressor schedules the $n_B$th packet to be uncompressed as part of the context refresh procedure. The scheduling of periodic context refresh packets is deterministic. The second factor arises from the fact that a WLSB encoded field can be decoded only if the number of consecutive decompression failures (since the last decompression success) is less than $w$. We summarize all the above considerations as

$$P(D(n_B) = 1 | \Psi^K, w, r) = \begin{cases} P(B(n_B) = 1), & n_B \in \{1, r+1, 2r+1, \ldots\}, \\ P(B(n_B) = 1) \Big[ P(C(n_B) = 0) + P(C(n_B) = 1) & \\ \quad \times \sum_{l_B = 0}^{w-1} P(L_B(j_B) = l_B, D(n_B - l_B - 1) = 1) \Big], & \text{otherwise.} \end{cases} \tag{22}$$

We note that the expression $P(L_B(j_B) = l_B, D(n_B - l_B - 1) = 1) = P(L_B(j_B) = l_B) \times P(D(n_B - l_B - 1) = 1 | B(n_B - l_B - 1) = 1)$ holds because the probability of decompression success at the $(n_B - l_B - 1)$th packet is independent of all future packet errors over Channel B. Therefore, expressing Eq. (22) in conditional probability with further simplification, we have a recursive definition

$$P^1_{D|\Psi^K,w,r,B}(n_B) \equiv P(D(n_B)=1|\Psi^K,w,r,B(n_B)=1)$$
$$= \begin{cases} 1, & n_B \in \{1, r+1, 2r+1, \ldots\}, \\ 1 - P(C(n_B)=1) & \\ \quad \times \left(1 - \sum_{l_B=0}^{w-1} P(L_B(j_B)=l_B) \times P^1_{D|\Psi^K,w,r,B}(n_B - l_B - 1)\right), & \text{otherwise.} \end{cases} \tag{23}$$

### 3.6. Performance metrics in new perspectives

We show that the modeling framework offers new perspectives on the three performance metrics defined in ROHC [2].

#### 3.6.1. Compression efficiency

The compression efficiency, or CE, is determined by how much the header sizes are reduced by the compression scheme. We show how it can be defined from our modeling framework.

For the scheme defined by the set of parameters $\{\Psi^K, w, r\}$, the mean compression success probability of the $j$th WLSB code $(b_j, o_f)$ is the time average of its compression success probability

$$\overline{C}_j = \begin{cases} \lim_{n_B\to\infty} \frac{1}{n_B} \sum_{i=1}^{n_B} P(C(i)=1|o_f, b_j, w), & j = 1,2,\ldots,K-1, \\ 1, & j = K. \end{cases} \tag{24}$$

where from Proposition 1, $\overline{C}_{K-1} = \overline{C}$ is also the mean probability of compression success for the codebook $\Psi^K$, and $\overline{C}_K = 1$ due to the fact there are no conditions for leaving a field uncompressed.

Note that we have defined the mean compression success probability in the form as shown in Eq. (24) for flexibility. In simulation, Eq. (24) can be evaluated by using a large number of samples ($n_A \to \infty$) and each $i$th term becomes an event with binary outcome (1 or 0). If both source and channel processes are ergodic in the limit $n_A \to \infty$, then Eq. (24) can also be evaluated from steady-state analytical expressions. It has already been shown that the channel process converges to steady-state probability, and is thus ergodic in the limit $n_A \to \infty$. We will present in Section 4 an IPID source model which also converges to ergodicity.

Due to the property that $V(o_f, b_i) \subset V(o_f, b_j)$ if $i < j$, The compression success event of each $j$th code is a superset of preceding codes. We thus obtain the probability of *using* the $j$th code as

$$U_j = \begin{cases} \overline{C}_j, & j = 1, \\ \overline{C}_j - \overline{C}_{j-1}, & 2 \leqslant j \leqslant K. \end{cases} \tag{25}$$

In the absence of context refreshes, the mean compressed size can be expressed as

$$\overline{b}' = \sum_{i=1}^{K-1} U_i b_i + U_K m + \eta, \tag{26}$$

where $\eta$ is the overhead incurred in discriminator bits. These are sometimes Huffman coded as part of packet format discriminators in ROHC-TCP, and $\eta$ can be approximated by the entropy of discriminator bits, i.e. $\eta \cong -\sum_{i=1}^{K} U_i \log_2 U_i$. In other cases, these bits are simply sent as is, and so $\eta = \lceil \log_2 K \rceil$. We assume that Huffman coding is used in all cases.

Factoring in the overhead incurred in the presence of context refreshes of period $r$, the mean compressed outcome becomes

$$\bar{b} = \frac{r-1}{r}\bar{b}' + \frac{1}{r}m \tag{27}$$

and we can then define the compression efficiency of a scheme as

$$\mathrm{CE}(\Psi^K, w, r) = m/\bar{b} = mr\left[m + (r-1)\left(\sum_{i=1}^{K-1} U_i b_i + U_K m + \eta\right)\right]^{-1}, \tag{28}$$

which takes on values in the range $\mathrm{CE} \geqslant 1$. We can see both from intuition and Eq. (28) that $\mathrm{CE}(\Psi^k, w, r)$ is a monotonically increasing function of $r$.

In the limit $r \to \infty$, the asymptotic upper limit of CE is expressed as

$$\mathrm{CE}_\infty(\Psi^K, w) = \lim_{r\to\infty} \mathrm{CE}(\Psi^K, w, r) = m\left[\sum_{i=1}^{K-1} U_i b_i + U_K m + \eta\right]^{-1}. \tag{29}$$

The above result plays an important role in the optimization of the codebook $\Psi^K = \{\{(b_i, o_f)\}_{i=1}^{K-1}, m\}$ in a scheme, as will be elaborated upon in Section 3.7. Finally, the definition of CE is non-unique. For example, another definition would be the ratio of the entropy to the mean compressed size.

### 3.6.2. Robustness

A robust scheme tolerates loss and residual errors on the link over which header compression takes place without losing additional packets or introducing additional errors in decompressed headers [2].

Because WLSB is the only mechanism in ROHC *preventing* damage propagation, instead of *helping recovery* from it, the robustness of a scheme can be seen from its $w$: a larger $w$ indicates a more robust scheme.

### 3.6.3. Compression transparency

The compression transparency, CT, is the extent to which a scheme prevents extra packet loss due to header compression, i.e. packet discards caused by invalid contexts. This can be obtained from the time average of conditional decompression success probability

$$\mathrm{CT}(\Psi^K, w, r) = \lim_{n_B\to\infty} \frac{1}{n_B} \sum_{i=1}^{n_B} P(D(i) = 1 | \Psi^K, w, r, B(i) = 1). \tag{30}$$

One disadvantage of the above expression and Eq. (23) is that it is dependent on the probability of compression success, which is in turn dependent on the source model. We can study a less complex relationship by finding the *minimum* compression transparency $\mathrm{CT}_{\min}$. Let the compression success probability be 1, i.e. $P(C(n_B) = 1) = 1$. The conditional decompression success probability is no longer dependent on the codebook, and Eq. (23) reduces to

$$\begin{aligned} P^1_{D|w,r,B}(n_B) &\equiv P(D(n_B) = 1 | w, r, B(n_B) = 1) \\ &= \begin{cases} 1, & n_B \in \{1, r+1, 2r+1, \ldots\}, \\ \sum_{l_B=0}^{w-1} P(L_B(j_B) = l_B) & \\ \quad \times P^1_{D|w,r,B}(n_B - l_B - 1), & \text{otherwise.} \end{cases} \end{aligned} \tag{31}$$

A result of this is that

$$\begin{aligned} &P^1_{D|w,r,B}(n_B) \leqslant P^1_{D|\Psi^K,w,r,B}(n_B) \\ &\therefore \mathrm{CT}_{\min}(w, r) \leqslant \mathrm{CT}(\Psi^K, w, r). \end{aligned} \tag{32}$$

Note that $\mathrm{CT}_{\min}$ becomes a close approximation of CT *if* the codebook is designed such that *high compression success probability* is achieved, i.e. $P(C(n_B) = 1) \approx 1\ \forall n_B = 1, 2, \ldots$. In this case, the compression transparency can be approximated independently of the source, Channel A and compressor processes. In most applications, a high CT is important because the cost of each extra packet loss is high. A high CE and low CT is in fact detrimental to overall performance because it does not make sense to compress packets into tiny sizes but lose most of them due to invalid contexts. We use $\mathrm{CT}_{\min}$ to guarantee the *desired level of performance* in our scheme optimization procedure.

### 3.7. The optimization of a scheme

#### 3.7.1. The goal of optimization

Given the source process $\{S(n_A)\}$ and channel processes $\{A(n_A)\}, \{B(n_B)\}$, the goal of optimization is to find the set of parameters $\{\Psi_{\text{opt}}^{K_{\text{opt}}}, w_{\text{opt}}, r_{\text{opt}}\}$ used by the compressor and decompressor processes $\{C(n_B)\}, \{D(n_B)\}$ achieving *at least* the desired level of compression transparency, $\text{CT}_{\text{des}}$, such that the compression efficiency is maximized.

We have used the notation $\Psi_{\text{opt}}^{K_{\text{opt}}}$ to denote the optimum codebook at the optimum size of $K_{\text{opt}}$ codes. For *any* codebook of $K$ codes in general, where $\Psi^K = \{\{(b_i, o_f)\}_{i=1}^{K-1}, m\}$ and $K-1 \leqslant m$, there can be a total of $\theta_K = \frac{m!}{(K-1)!(m-K+1)!}$ different codebooks each with a unique combination of parameters. This is due to the fact that to have any compression gains, i.e. CE is in the range $\text{CE} \geqslant 1$, all $b_i$'s must be in the range $0 \leqslant b_i \leqslant m-1$. Furthermore, all $b_i$'s are unique in the codebook. For any particular fixed $K$, we denote the entire set codebooks of $K$ codes by $\{\Psi_j^K : j = 1, 2, \ldots, \theta_K\}$.

#### 3.7.2. The optimization procedure

We first derive a result which will be used as part of our optimization procedure:

**Proposition 2.** *For any fixed $w$ and $r$, the optimum codebook $\Psi_{\text{opt}}^{K_{\text{opt}}}(w)$ maximizing the asymptotic compression efficiency, $\text{CE}_\infty(\Psi^K, w)$ also maximizes the compression efficiency, $\text{CE}(\Psi^K, w, r)$.*

**Proof.** The optimum codebook at a fixed $w$, $\Psi_{\text{opt}}^{K_{\text{opt}}}(w)$, maximizes the asymptotic compression efficiency, i.e. $\text{CE}_\infty(\Psi_{\text{opt}}^{K_{\text{opt}}}(w), w) = \max_{K\in[1,m+1], j\in[1,\theta_K]}\{\text{CE}_\infty(\Psi_j^K, w)\}$. We know from Eqs. (27)–(29) that $\frac{1}{\text{CE}(\Psi^K,w,r)} = (\frac{r-1}{r})\frac{1}{\text{CE}_\infty(\Psi^K,w)} + \frac{m}{r}$. This mapping from $\text{CE}_\infty^{-1}(\Psi^K, w)$ to $\text{CE}^{-1}(\Psi^K, w, r)$ is affine when $r$ is fixed and thus $\text{CE}(\Psi_{\text{opt}}^{K_{\text{opt}}}(w), w, r) = [(\frac{r-1}{r})\frac{1}{\max_{K\in[1,m+1],j\in[1,\theta_K]}}\{\text{CE}_\infty(\Psi_j^K, w)\} + \frac{m}{r}]^{-1} = \max_{K\in[1,m+1],j\in[1,\theta_K]}\{\text{CE}(\Psi_j^K, w, r)\}$. □

We now explain the idea behind our optimization procedure. For each fixed $w$, we can find the optimum codebook $\Psi_{\text{opt}}^{K_{\text{opt}}}(w)$ which maximizes $\text{CE}_\infty(\Psi^K, w)$. From Proposition 2, we know that the resultant codebook at each $w$ is also optimum for $\text{CE}(\Psi^K, w, r)$. Next, if we know the set of $(w, r)$ pairs $\zeta$ such that the condition $\text{CT}_{\min}(w, r) \geqslant \text{CT}_{\text{des}}$ is satisfied, then regardless of the codebook used, the compression transparency criterion in the goal of optimization will be satisfied in $\zeta$, i.e. $\text{CT}(\Psi^K, w, r) \geqslant \text{CT}_{\min}(w, r) \geqslant \text{CT}_{\text{des}}\ \forall (w, r) \in \zeta$. Finally, by finding the optimum pair $(w_{\text{opt}}, r_{\text{opt}})$ in $\zeta$ which maximizes $\text{CE}(\Psi_{\text{opt}}^{K_{\text{opt}}}(w), w, r)$, we will have achieved the goal of optimization since $\Psi_{\text{opt}}^{K_{\text{opt}}}(w_{\text{opt}})$, $w_{\text{opt}}$ and $r_{\text{opt}}$ are found. We therefore present a three-step approach to achieving scheme optimization:

*Step 1.* For *each* given $w$, find the optimum codebook, $\Psi_{\text{opt}}^{K_{\text{opt}}}(w) = \{\{(b_i, o_f)\}_{i=1}^{K_{\text{opt}}-1}, m\}$ such that $\text{CE}_\infty \times (\Psi_{\text{opt}}^{K_{\text{opt}}}(w), w) = \max_{K\in[1,m+1], j\in[1,\theta_K]}\{\text{CE}_\infty(\Psi_j^K, w)\}$.

*Step 2.* Add all parameter pairs $(w, r)$ that satisfies the condition $\text{CT}_{\min}(w, r) \geqslant \text{CT}_{\text{des}}$ to the set $\zeta$, i.e. $(w, r) \in \zeta$ if $\text{CT}_{\min}(w, r) \geqslant \text{CT}_{\text{des}}$.

*Step 3.* Find the optimum parameter pair $(w_{\text{opt}}, r_{\text{opt}})$ such that $\text{CE}(\Psi_{\text{opt}}^{K_{\text{opt}}}(w_{\text{opt}}), w_{\text{opt}}, r_{\text{opt}}) = \max_{(w,r)\in\zeta}\{\text{CE}(\Psi_{\text{opt}}^{K_{\text{opt}}}(w), w, r)\}$.

Note that we have presented a conceptual optimization *procedure* rather than an *algorithm*. An efficient algorithm can be developed to achieve the same conceptual outcome of our procedure. The design of an efficient algorithm is however outside the scope of this paper. Note also that we have substantially reduced the parameter space by using a constant offset in our codebook $\Psi^K = \{\{(b_i, o_f)\}_{i=1}^{K-1}, m\}$. Thus, the optimum codebook obtained in Step 1 is optimum only for a particular fixed offset.

### 3.8. Modeling different source and deployment scenarios

Different deployment scenarios can be modeled by varying the channel processes $\{A(n_A)\}, \{B(n_B)\}$. Note that (i) our modeling framework models the data flow in a single direction, (ii) Channel A is the channel

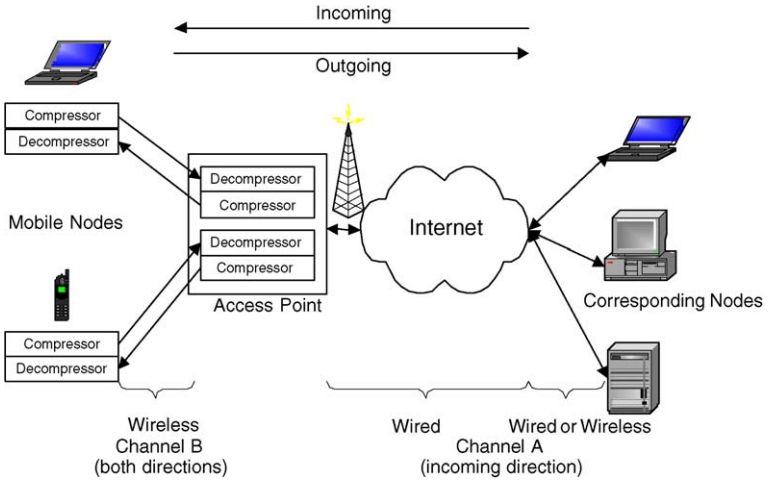


Fig. 5. Header compression deployment over the last hop.

between the source and compressor and (iii) Channel B is the channel between the compressor and decompressor.

Fig. 5 illustrates the common 'last hop' deployment of header compression. We define 'incoming' as the direction of packet flow towards the clients and 'outgoing' to be in the opposite direction. Our modeling framework is easily adapted to this deployment scenario. Regardless of the direction of flow, Channel B is wireless. In the 'outgoing' direction, Channel A is a perfect channel (because the source and compressor are co-located); in the 'incoming' direction, we have a wired/wireless/hybrid Channel A.

In another scenario where both the corresponding nodes are mobile, or when header compression is deployed over an intermediate wireless hop, then both Channels A and B are simply wireless channels.

Since wireless channels are affected by the effects of fading due to mobility, the effect of mobility speed can be studied by tuning the channel models for different speeds. Different mobility speeds arise due to different deployment scenarios (e.g. header compression nodes are on a moving vehicle versus a walking pedestrian).

Finally, different source scenarios can be modeled by tuning the model for the source process, $\{S(n_A)\}$ or $\{\Delta(n_A)\}$. We present such a model for IPID in the next section.

## 4. The IPID source model

The IPID field has been chosen to illustrate the concept of a source model, because it is one of the few header fields with complicated behavior in header compression schemes, and the *only* commonly used field with complicated behavior in the IP protocol. We first present the structure of our source model in detail. We then show that it can be built to model real-world traffic traces and verify its accuracy.

### 4.1. Structure of source model

Our approach is to develop a model for the discrete stochastic process $\{\Delta(n_A)\}$ generating IPID deltas $\{\delta(n_A)\}$.

Consider a source generating $N$ flows concurrently. Let each flow $f$ be represented by a Markov chain $\{(f,1),(f,2),\ldots,(f,j),\ldots\}$ where $j$ is the number of *consecutive packets* in flow $f$ sent by the source *without switching to another flow*. In a state $(f,j)$, the source is in the process of transmitting the $j$th consecutive packet from flow $f$. To transmit the next packet, it either makes a transition to the next state of the same flow $(f,j+1)$ or to the first state of another flow $(f',1)$, such that $f' \in [1,N]$, $f' \neq f$ At each transition, the shared IPID is incremented. For the case of three flows, i.e. $N=3$, we can visualize the IPID model as shown in Fig. 6.

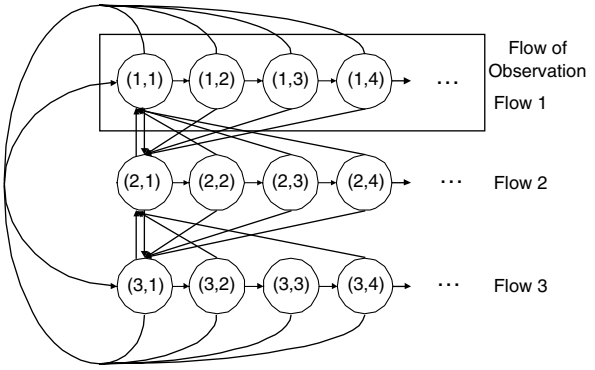


Fig. 6. IPID Markov model for three concurrent connections ($N = 3$) and flow 1 is the flow of observation ($f_o = 1$).

Let $(f,j)$ and $(f',j')$ be any two states in the model and $q_{(f,j)}^{(f',j')}$ denote the transition probability from state $(f,j)$ to $(f',j')$. We can make the following general characterizations for any outward transitions from $(f,j)$:

$$q_{(f,j)}^{(f',j')} = \begin{cases} q_{(f,j)}^{(f,j+1)} & \text{if } f' = f, \text{ where } q_{(f,j)}^{(f,j+1)} \in [0,1), \\ q_{(f,j)}^{(f',1)} & \text{if } f' \neq f, \text{ where } q_{(f,j)}^{(f',1)} \in [0,1], \\ 0, & \text{otherwise.} \end{cases} \tag{33}$$

The notion of *N concurrent* flows advocates that the transition to the next state of the same flow cannot be made with certainty. Therefore, $q_{(f,j)}^{(f,j+1)}$ is in the range $[0,1)$ as indicated in Eq. (33). We also adopt the following notations for compactness:

$$Q(f,j) = \begin{cases} 1, & j = 0, \\ \prod_{i=1}^{j} q_{(f,i)}^{(f,i+1)}, & \text{otherwise.} \end{cases} \tag{34}$$

It can be seen from the structure of the model that it is indecomposable (there is only one essential state set) and aperiodic. Thus, given sufficient time, it converges to a stationary distribution.

Define $p(f,j)$ as the stationary probability of being in state $(f,j)$. The stationary probability of any state $(f,j)$ which is not the head of its flow can be expressed as

$$p(f,j) = p(f,1)Q(f,j-1), \quad j > 1. \tag{35}$$

Thus, we only need to know each $p(f,1) \forall f = 1,2,\ldots,N$. $p(f,1)$ can be obtained from the balance equation:

$$p(f,1) = \sum_{\substack{k=1 \\ k \neq f}}^{N} \sum_{j=1}^{\infty} p(k,j) q_{(k,j)}^{(f,1)}, \quad \forall f \in [1,N]. \tag{36}$$

Also, we know that all state probabilities must sum up to 1, which can be simply expressed as

$$\sum_{k=1}^{N} \sum_{j=1}^{\infty} p(k,j) = 1. \tag{37}$$

Using Eqs. (35)–(37), we can easily solve the stationary state probabilities.

We are interested in deriving $P(\Delta(n_A) = \delta(n_A))$ in terms of Markov state probabilities. Upon convergence, as $n_A \to \infty$, the stationary state probabilities are fixed and the problem reduces to determining the expression for $P(\Delta = \delta)$ in terms of the stationary state probabilities.

Defining $\mathscr{S}$ the current state within the flow of observation, we can express $P(\Delta = \delta)$ in terms of its conditional probabilities

$$P(\Delta=\delta)=\frac{1}{p(f_o)}\sum_{i=1}^{\infty}P(\Delta=\delta|\mathscr{S}=(f_o,i))p(f_o,i)=\frac{p(f_o,1)}{p(f_o)}\left[\sum_{i=1}^{\infty}Q(f_o,i-1)P(\Delta=\delta|\mathscr{S}=(f_o,i))\right], \tag{38}$$

where $p(f_o)=\sum_{j=1}^{\infty}p(f_o,j)$ is the probability that a packet belongs to the flow of observation $f_o$. The complexity of the problem lies in the expression $P(\Delta=\delta|\mathscr{S}=(f_o,i))$.

Note that $\delta$ is actually the *number of transitions* made between two *observable states*. To the observer, an observation, $\delta$ is made *only when* there is a transition *into* any state in $f_o$. Furthermore, the first $(\delta-1)$ transitions *since the last observation* must occur *outside* $f_o$. The remaining transition must be back to $f_o$ (so as to make the observation $\delta$).

The case of $\delta=1$ is a special case because there is no transition out of $f_o$, i.e. the next transition must be to the next state of the same flow. If $(f_o,i)$ is the current state, the next state must be $(f_o,i+1)$. Therefore, we can see that

$$P(\Delta=\delta|\mathscr{S}=(f_o,i))=q_{(f_o,i)}^{(f_o,i+1)},\quad \text{if } \delta=1. \tag{39}$$

For $\delta\geqslant 2$, we only know that the first transition is *out* of $f_o$, and the last transition is *back* to $(f_o,1)$. At high $N$ and $\delta$ the number of possible paths increases tremendously and it is difficult to obtain a general expression for $P(\Delta=\delta|\mathscr{S}=(f_o,i))$ in closed form. Instead, we can evaluate $P(\Delta=\delta|\mathscr{S}=(f_o,i))$ in the range $\delta\geqslant 2$ with the help of a recursive function.

We define the recursive function $F((f,i),T,f_o)$, described as "the probability of making $T-1$ transitions *outside* $f_o$ before making the final transition back to $(f_o,1)$, given the current state is $(f,i)$". This function can thus be defined as

$$F((f,i),T,f_o)=\begin{cases} q_{(f,i)}^{(f_o,1)}, & \text{if } T=1,\\ \left[\sum\limits_{\substack{f'=1\\ f'\neq f_o,f}}^{N} q_{(f,i)}^{(f',1)}F((f',1),T-1,f_o)+q_{(f,i)}^{(f,i+1)}F((f,i+1),T-1,f_o)\right], & \text{otherwise.}\end{cases} \tag{40}$$

$P(\Delta=\delta|\mathscr{S}=(f_o,i))$ can be obtained in terms of $F$ as follows:

$$P(\Delta=\delta|\mathscr{S}=(f_o,i))=\sum_{\substack{f=1\\ f\neq f_o}}^{N} q_{(f_o,i)}^{(f,1)}F((f,1),\delta-1,f_o),\quad \delta\geqslant 2. \tag{41}$$

Summarizing the above results, we can express $P(\Delta=\delta)$ as

$$P(\Delta=\delta)=\begin{cases}\dfrac{p(f_o,1)}{p(f_o)}\left[\sum\limits_{i=1}^{\infty}Q(f_o,i)\right], & \delta=1,\\ \dfrac{p(f_o,1)}{p(f_o)}\left[\sum\limits_{i=1}^{\infty}Q(f_o,i-1)\sum\limits_{\substack{f=1\\ f\neq f_o}}^{N} q_{(f_o,i)}^{(f,1)}F((f,1),\delta-1,f_o)\right], & \delta\geqslant 2.\end{cases} \tag{42}$$

Eq. (42) can be plugged into the modeling framework at Eq. (19) for the analysis of the performance of a scheme designed to compress the IPID. Since it also models the way packets are generated from a source handling multiple concurrent flows, it can also be used in other applications.

Note that different source scenarios can arise causing IPID source behavior to be different. A busy source generating a large number of flows can be intuitively modeled using a high $N$ model. Conversely, a naive source generating only a single, non-concurrent flow is easily modeled with $N=1$. In Section 4.3, we build a two-flow model for an average source and a 10-flow model for the busy source.

Table 1
Variations in controlled environments

| Parameter | Parameter space |
|---|---|
| No. of concurrent flows | 2–4 |
| Type of channel | wired (802.3) or wireless (802.11b) |
| User application | web browser, remote terminal, LAN gaming, file downloads, file sharing |
| Protocol headers | {HTTP[a], SSH[b], proprietary, FTP[c], NetBIOS[d]} over TCP/IP |
| Nature of payload | Data or acknowledgments |

[a] HyperText Transfer Protocol.
[b] Secure SHell.
[c] File Transfer Protocol.
[d] Network Basic Input Output System.

### 4.2. Verification of model

Our model verification approach is to generate from a source terminal a large number of packets from a known number of concurrent flows in controlled environments and capture them right at the source. This ensures that a large number of outgoing packet samples is available for obtaining the Markov transition parameters of the model. Using packet traces, we also verify our assumption in Section 3.4 that the occurrence of wraparound is rare. Having built the model from the packet traces, the distribution $P(\Delta = \delta)$ is then obtained analytically from the model for comparison with the histogram of IPID deltas found in the traces.

Using source terminals running Microsoft Windows, different controlled environments were explored, and our parameter space includes the number of concurrent flows, type of channels, type of applications, type of protocol headers, and the nature of payloads. These variations are tabulated in Table 1.

After converting the IPID values in the traces into network byte order, we find that the distributions obtained from our IPID model nicely track the IPID distributions obtained from traces in all of the above experiments. We show the distribution comparisons for the case of FTP file download over wireless Ethernet in Fig. 7 and the case of HTTP file download acknowledgments over wired Ethernet in Fig. 8.

We note from Fig. 7 that the distribution obtained from our model is almost identical to that in the trace. The same level of resemblance is not found in Fig. 8. Examining packets in that trace, we find that for HTTP especially, two consecutive packets generated from the source *may not* carry an increment of +1. Furthermore, packets exhibiting such behavior characteristically show unusually long timestamp lags. This suggests that such packets were interrupted before they could be generated completely. In spite of this, the assumption of +1 increment per packet is usually true and Fig. 8 shows that the distribution obtained with this assumption closely tracks that from traces.

### 4.3. Constructing a real-world source model

In the previous section we have only verified the concept of a source model in controlled environments. We desire to build a model for the average source in the real world. Based on the IPID delta probability distributions from packets in real traffic, our objective is to find a model which approximates the source at the zeroth as well as higher orders. To do this, we have obtained a trace, TCP080903out which captures 266831 outgoing TCP packet headers from the Institute of Infocomm Research LAN over a half-hour interval.

Essentially, we are trying to obtain the Markov transition parameters from the probability distribution, i.e. performing the reverse of what we did in the previous section. We can see from Eq. (42) that this is a non-trivial task due to the infinite number of states and the unknown (and furthermore non-constant) number of concurrent flows, $N$. Naturally, this requires some assumptions and approximations to be made. We first reduce the search space by truncating the chain of states in each flow. We further assume that the average source can be modeled with 2 concurrent flows, i.e. $N = 2$. We then show how a real-world source model can be built.

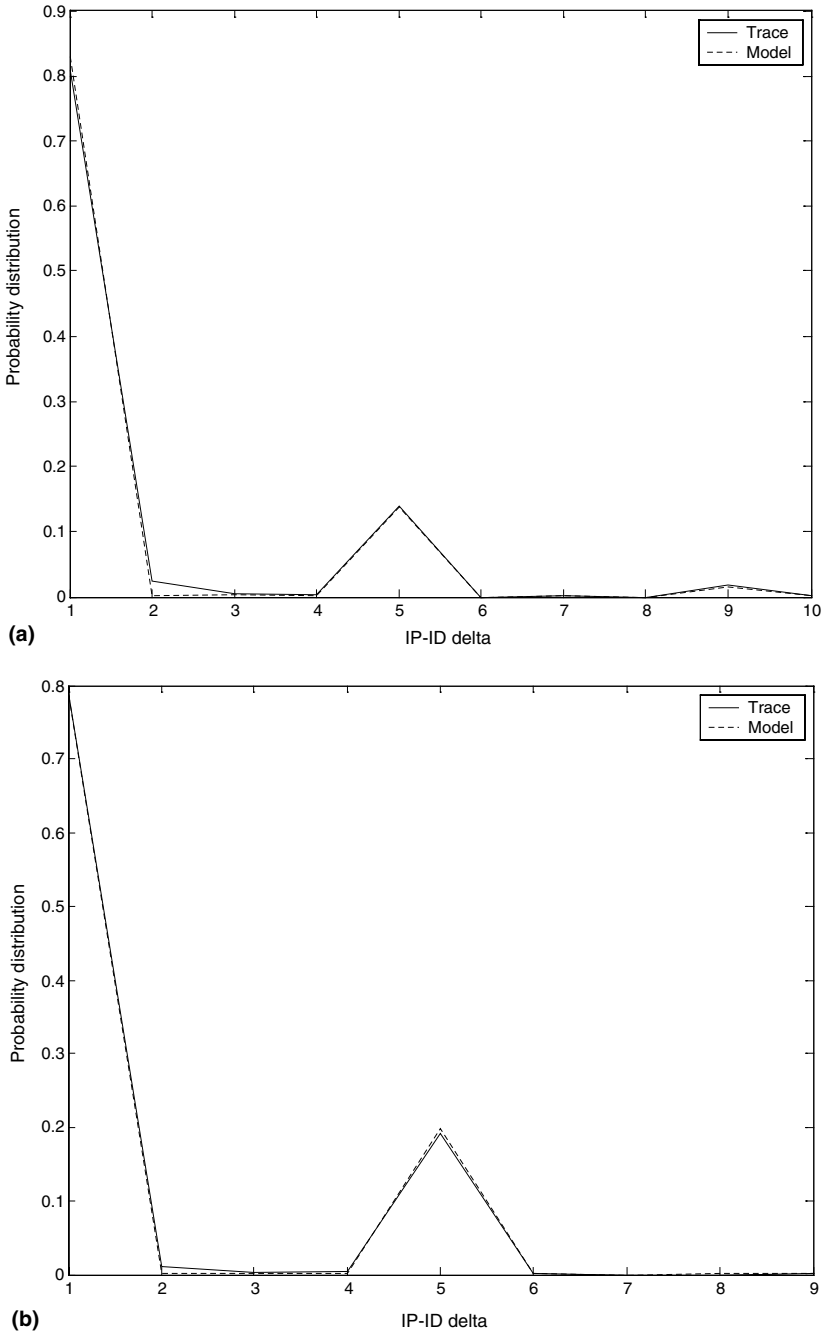


Fig. 7. $P(\Delta = \delta)$ for four concurrent flows, generated by FTP file downloads over wireless Ethernet. Flows of observation $f_o = 1$ (a) and $f_o = 2$ (b) are data flows. Distributions from control flows are not obtained due to small numbers of control packets.

### 4.3.1. Truncation

To reduce the complexity of the model, our aim is to truncate the number of states in each flow to a small finite number with little sacrifice in accuracy. To avoid deriving all our earlier source model equations again, we achieve this in two steps: We first approximate the original infinite-states model with a simpler infinite-states model. The approximated infinite-states model is then mapped to an equivalent finite-states model. Using a single flow as an example, this is illustrated in Fig. 9.

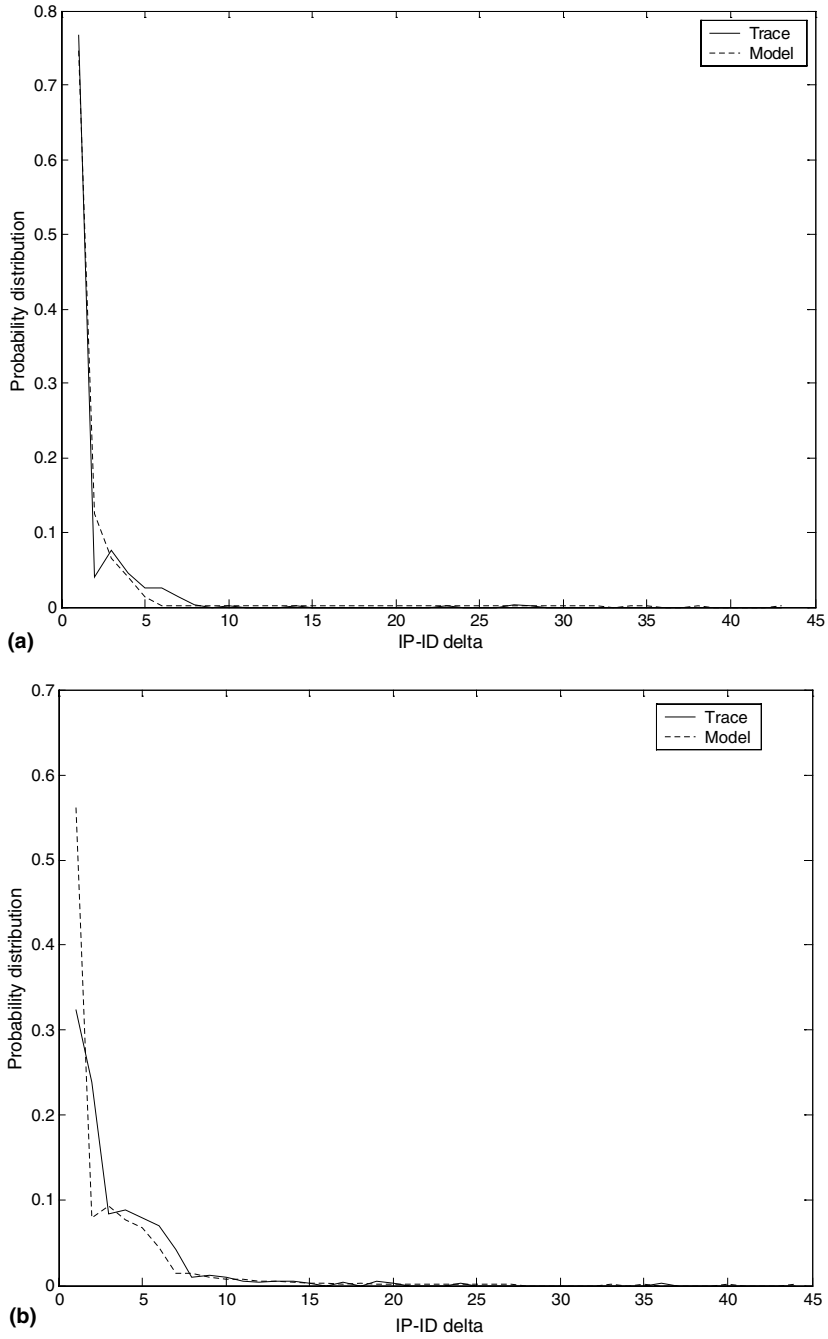


Fig. 8. $P(\Delta = \delta)$ for two concurrent flows, generated by HTTP file download ACKs over wired Ethernet. Flows of observation are $f_o = 1$ (a) and $f_o = 2$ (b).

For each chain of states representing a flow $f$, we first approximate the remaining transition probabilities beyond a certain threshold state, $h_f$, as an averaged constant, $q$. Then the approximation of $Q(f,j)$ defined in Eq. (34) is

$$\hat{Q}(f,j) = \begin{cases} Q(f,j), & j < h_f, \\ q^{j-h_f+1} Q(f,h_f-1), & j \geqslant h_f, \end{cases} \tag{43}$$

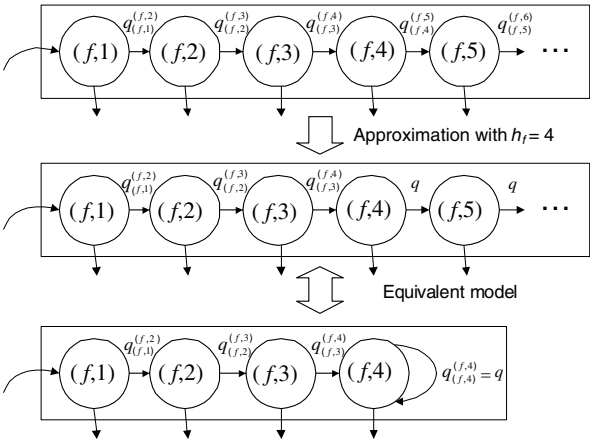


Fig. 9. Illustration of model truncation.

and the approximation error can be defined as

$$\varepsilon(f,j) = |Q(f,j) - \hat{Q}(f,j)|. \tag{44}$$

It can be easily shown that $\lim_{j\to\infty}\varepsilon(f,j) = 0\ \forall h_f$, due to the fact that $Q(f,j)$ is in the range $[0,1)\ \forall f = 1,2,\ldots,N$ (see Eq. (33)). This means that the approximation error decreases to zero if the approximated state is far from the head of its flow, regardless of the threshold value $h_f$. However, in general $h_f$ remains a tradeoff between model complexity and approximation error.

As illustrated in Fig. 9, the approximated model of infinite states in Eq. (43) can be mapped to an equivalent model with $h_f$ states in each flow $f$, such that the tail state of the flow transits to itself with probability $q_{(f,h_f)}^{(f,h_f)} = q$. To continue using our earlier results, the following corollary is useful for mapping between the approximated model of infinite states and its equivalent model of finite states:

**Corollary 1.** *If the approximated model of infinite states has an equivalent model of finite states, the following mapping holds*:

$$\sum_{j=h_f}^{\infty}\hat{Q}(f,j) = \frac{Q(f,h_f-1)q_{(f,h_f)}^{(f,h_f)}}{1-q_{(f,h_f)}^{(f,h_f)}}.$$

**Proof.** This result follows from Eq. (43) and can be proved easily. □

*4.3.2. Two-flow assumption*

For the case of two concurrent flows, i.e. $N = 2$, Eq. (42) can be reduced into a simpler closed form. This is due to the fact that there are only two paths out of each state (see Eq. (33)). Furthermore, given any $\delta \geqslant 2$ there is only a single deterministic path to follow. As such, there is no need to express $P(\Delta = \delta|\mathscr{S} = (f_o, i))$ in terms of the recursive function $F$. Let the two flows be $f_o$ and $f_1$ where $f_o$ is the flow of observation. We obtain a simpler form of Eq. (42):

$$P(\Delta = \delta) = \frac{p(f_o,1)Q(f_1,\delta-2)(1-q_{(f_1,\delta-1)}^{(f_1,\delta)})}{p(f_o)}, \quad \delta \geqslant 2. \tag{45}$$

The derivation of Eq. (45) is shown in Appendix A.

*4.3.3. Resultant real-world source model*

We now apply our two-flow assumption and truncation technique and show how the model parameters can be obtained from the probability distribution in the trace. Let the unknown number of states in each flow be $h_o$

and $h_1$ respectively. Applying the truncation approximation to the two-flow result in Eq. (45), we can isolate flow $f_1$ transition probabilities by obtaining the ratios of consecutive delta probabilities:

$$\frac{\hat{P}(\Delta=\delta+1)}{\hat{P}(\Delta=\delta)}=\begin{cases}\dfrac{q^{(f_1,\delta)}_{(f_1,\delta-1)}(1-q^{(f_1,\delta+1)}_{(f_1,\delta)})}{1-q^{(f_1,\delta)}_{(f_1,\delta-1)}}, & 2\leqslant\delta\leqslant h_1,\\ q^{(f_1,h_1)}_{(f_1,h_1)}, & \delta\geqslant h_1+1.\end{cases} \tag{46}$$

Estimating delta probability ratios from the trace, all flow $f_1$ transition probabilities can be obtained by solving the set of equations in Eq. (46) recursively.

Fig. 10 shows the delta probability ratios obtained from the trace, as well as the number of packets available at each delta value. We observe that the probability ratio gets increasingly jittery as delta increases. The reason for that is attributed to the decreasing number of packet samples available as delta increases, as shown in the bottom portion of Fig. 10. Fig. 10 also reveals that the probability ratio increases quickly at small deltas and remains relatively constant thereafter. This agrees well with Eq. (46) where the probability ratio remains constant at $q^{(f_1,h_1)}_{(f_1,h_1)}$ for $\delta\geqslant h_1+1$. We choose $h_1=19$ and obtain $q^{(f_1,h_1)}_{(f_1,h_1)}$ from the ratio mean for $\delta\geqslant h_1+1$. Solving Eq. (46) recursively, we then obtain the entire set of transition probabilities in flow $f_1$. The values obtained are shown in Table 2.

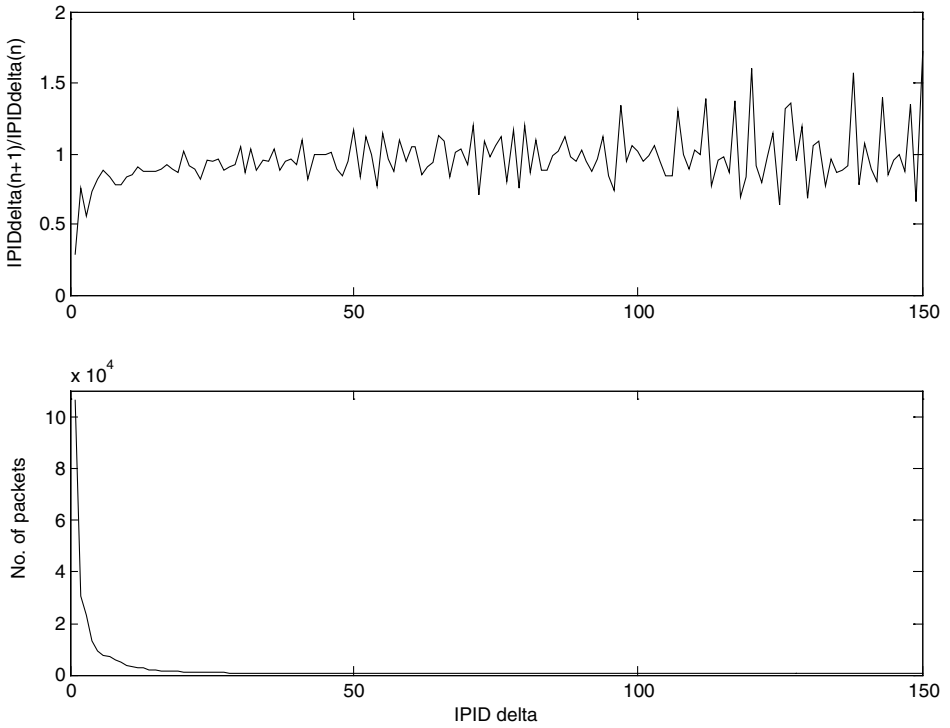


Fig. 10. Estimates of delta probability ratios obtained from trace (top) and corresponding number of packet samples (bottom).

Table 2
Markov model parameters for state $(f,j)$

| | $j=1$ | $j=2$ | $j=3$ | $j=4$ | $j=5$ | $j=6$ | $j=7$ | $j=8$ | $j=9$ | $j=10$ |
|---|---|---|---|---|---|---|---|---|---|---|
| $f=f_o$ | 0.263 | 0.3082 | 0.5783 | 0.6554 | 0.7124 | 0.7665 | 0.8209 | 0.8397 | 0.8297 | 0.96 |
| $f=f_1$ | 0.7912 | 0.8005 | 0.8606 | 0.8813 | 0.8891 | 0.8893 | 0.8958 | 0.9086 | 0.9208 | 0.9281 |
| | $j=11$ | $j=12$ | $j=13$ | $j=14$ | $j=15$ | $j=16$ | $j=17$ | $j=18$ | $j=19$ | $j=20$ |
| $f=f_o$ | – | – | – | – | – | – | – | – | – | – |
| $f=f_1$ | 0.9338 | 0.9361 | 0.9403 | 0.9446 | 0.9486 | 0.9518 | 0.9532 | 0.956 | 0.96 | – |

We also exploit another statistical characteristic of the trace to obtain flow $f_o$ transition parameters. Recall from the comments on Eq. (18) that a good source model should also approximate the high-order behavior of real sources, as this affects the compressibility. Therefore, our approach is to obtain flow $f_o$ transition parameters from the high-order probability distributions in the trace.

At steady state, the $n$th order probability distribution can be defined and expressed in the following form:

$$\gamma_n = \hat{P}(\Delta(n_A) = 1 | \Delta(n_A - n) = 1, \ldots, \Delta(n_A - 1) = 1) = \frac{\alpha_n}{1 - q^{(f_o,h_o)}_{(f_o,h_o)} + \alpha_n}, \quad \text{where } n \geqslant 1 \quad \text{and}$$

$$\alpha_n = \begin{cases} q^{(f_o,n+2)}_{(f_o,n+1)} \left[ (1 - q^{(f_o,h_o)}_{(f_o,h_o)}) \left( 1 + \sum_{j=n+2}^{h_o-1} \prod_{i=n+2}^{j} q^{(f_o,i+1)}_{(f_o,i)} \right) \right. \\ \quad \left. + q^{(f_o,h_o)}_{(f_o,h_o)} \prod_{i=n+2}^{h_o-1} q^{(f_o,i+1)}_{(f_o,i)} \right], & h_o \geqslant 4 \text{ and } 0 \leqslant n \leqslant h_o - 3, \\ q^{(f_o,n+2)}_{(f_o,n+1)}, & n = h_o - 2, \\ q^{(f_o,h_o)}_{(f_o,h_o)}, & n \geqslant h_o - 1. \end{cases} \tag{47}$$

The derivation of Eq. (47) is shown in Appendix B. By estimating each $\gamma_n$ from the trace and solving Eq. (47) recursively, we can obtain all $q^{(f_o,i+1)}_{(f_o,i)}$ in the range $2 \leqslant i \leqslant h_o - 1$. The remaining transition probability at $i = 1$, $q^{(f_o,2)}_{(f_o,1)}$, can be found using the following relationship:

$$\alpha_0 = (1 - q^{(f_o,h_o)}_{(f_o,h_o)}) \left( \frac{1 - q^{(f_1,2)}_{(f_1,1)}}{\hat{P}(\Delta = 2)} - 1 \right). \tag{48}$$

The result $q^{(f_o,h_o)}_{(f_o,h_o)} = \gamma_n, n \geqslant h_o - 1$ in Eq. (47) requires high-order statistics beyond the $n$th order in the trace to be constant. From Fig. 11, we verify that this is indeed the case as $n \to 20$ and $n \geqslant 21$. In the region $n \leqslant 20$, the

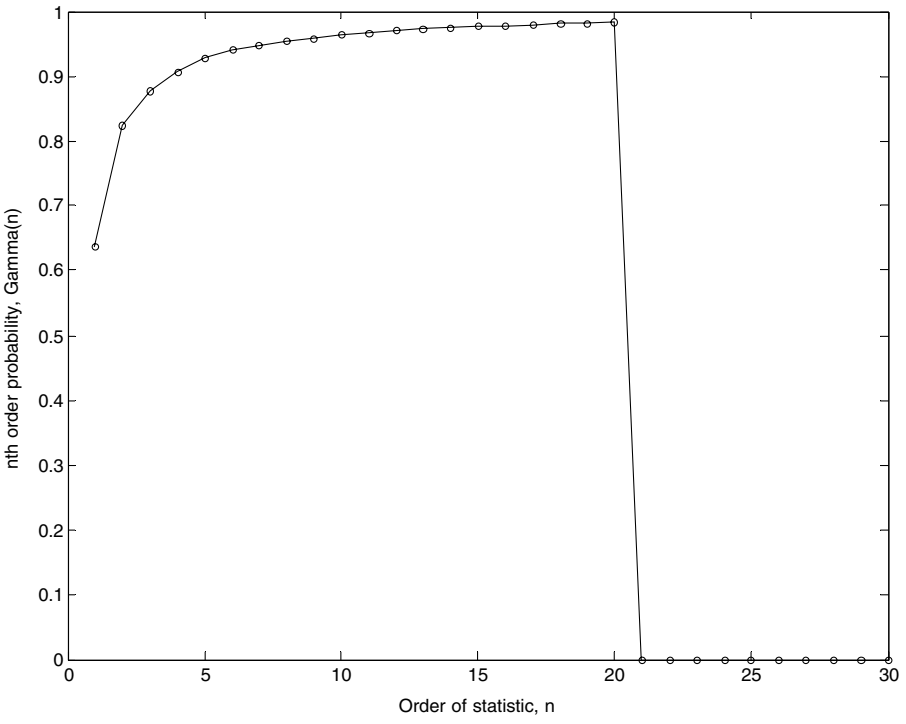


Fig. 11. The estimate of the $n$th order probability distribution $\gamma_n$ obtained from packet trace.

probability that the next packet generated comes from the same flow (given that the last $n$ packets also came from the same flow) increases asymptotically to 1. The lack of an uninterrupted series of 22 or more packets of the same flow causes the abrupt drop to a constant zero for $m \geqslant 21$.

Based on the above characteristic, we can either model flow $f_o$ with around 10 states with $q_{(f_o,h_o)}^{(f_o,h_o)} \approx 1$, or obtain an exact 22-state model for flow $f_o$ where $q_{(f_o,h_o)}^{(f_o,h_o)} = 0$. However, we adopt the 10-states model because we find that the abrupt drop to zero in the 22-state model coupled with the two-flow ($N = 2$) assumption produces a worse fit to the trace distribution compared to the 10-state model.

Table 2 shows the resultant parameters of the entire model with the transition probabilities in $f_o$ and $f_1$ combined. The zeroth order probability distribution obtained from this model is almost identical to the trace distribution as shown in Fig. 12.

Fig. 12 shows that the trace distribution is essentially heavy-tailed and has been truncated to show the fit at small deltas. To observe the closeness-of-fit at high deltas, we show the cumulative probabilities on a log scale in Fig. 13. The same figure also shows the distribution comparison at high orders using Eqs. (18) and (24) (setting $o_f = -1$, since IPID is increasing). Note that this is possible because the $n$th order cumulative probability of compression success can be obtained using a window size of $(w - 1)$ at the compressor with perfect Channel A. Fig. 13 shows that the model distributions track the high-order distributions and heavy-tail characteristic of the trace rather well. However, the trace distribution is slightly more heavy-tailed. This limit is imposed by our two-flow assumption and truncation approximation. However, given the model simplicity, we consider this a good tradeoff.

Fig. 14 shows the number of instantaneous concurrent flows generated from a real source. Interestingly, the case of 2 concurrent flows seems to be rather common. We note also that a source may experience short periods of extreme business, seen in the form of spikes, where large numbers of flows are generated.

Our two-flow model cannot match the heavy-tail of the trace distribution exactly mainly because the number of concurrent flows at the source in real life is a *non-constant*. The heavy-tail portion is therefore contributed by busy sources generating large numbers of concurrent flows. To verify that this concept is sound, we

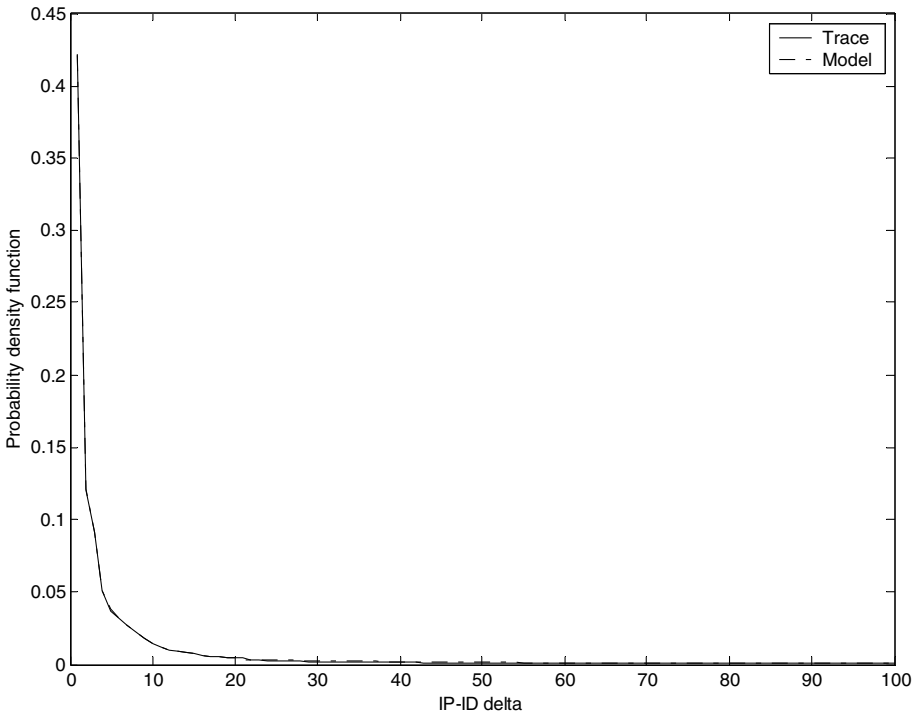


Fig. 12. Comparison of IPID delta distribution between model and trace. The trace distribution is heavy-tailed and is truncated to show the fit at small deltas.

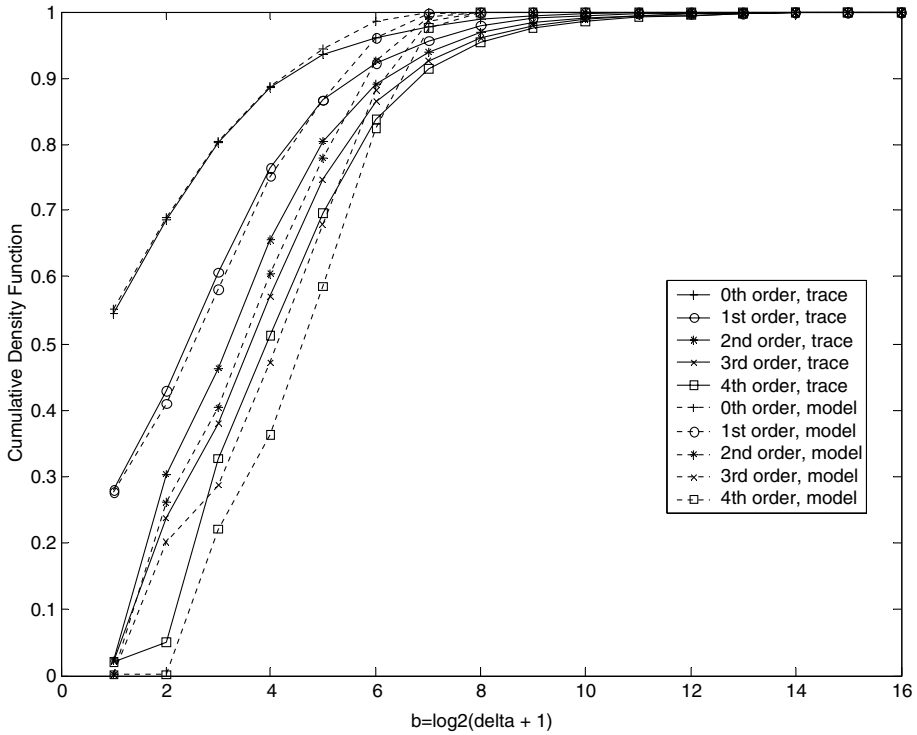


Fig. 13. Comparison of IPID delta cumulative distributions between trace and model on log scale from the zeroth order to the fourth order.

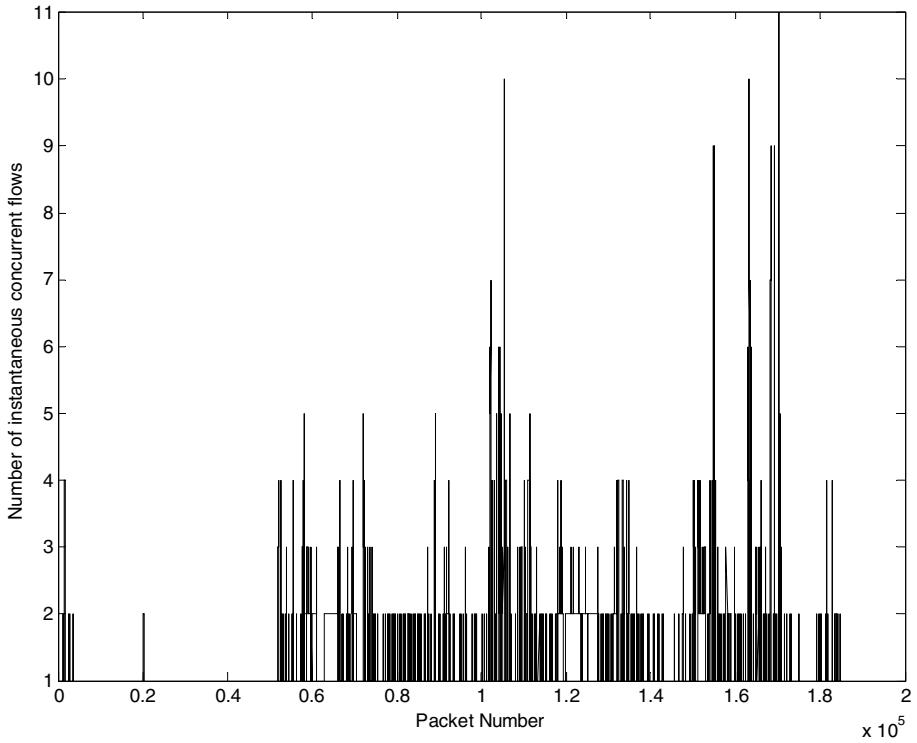


Fig. 14. Number of concurrent flows generated.

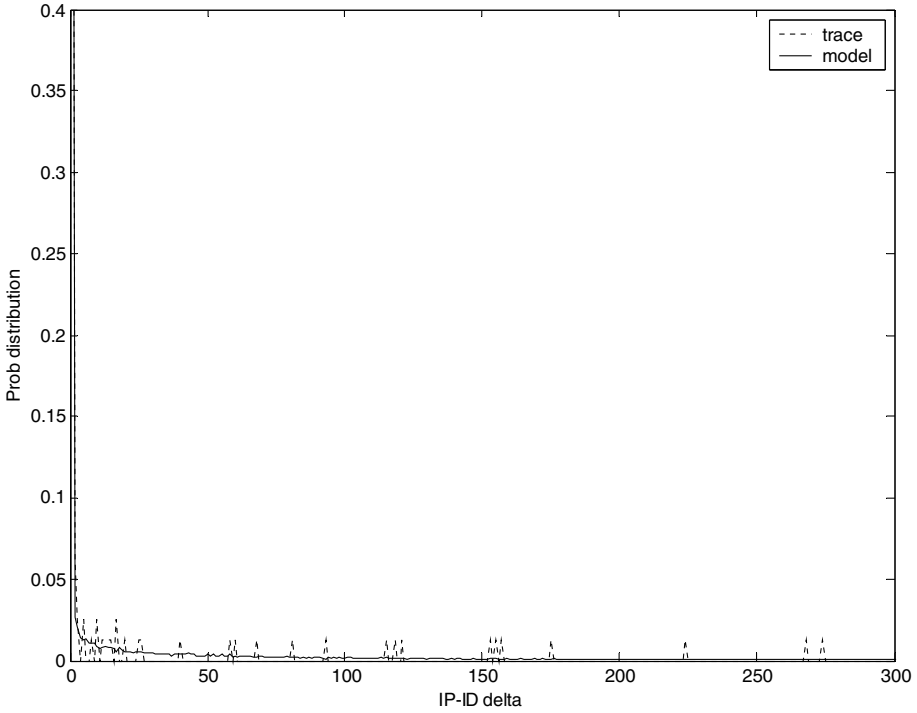


Fig. 15. Comparison of delta distribution from 10-flow model with a heavy-tailed flow in trace. Spikes are seen in the trace distribution due to limited resolution from in limited number of samples for a single flow.

extended our two-flow model to a 10-flow model. This is achieved by duplicating five copies of each chain of Markov states in the two-flow model and retaining the transition probabilities down each chain. In Fig. 15, we compare the distribution from the 10-flow model with a particularly heavy-tailed flow in the trace. Note that small spikes are observed from the trace distribution due to limited resolution from small number of packet samples in a single flow. Regardless of this, both distributions share the characteristics of a single large spike at $\delta = 1$ which diminishes to near zero at $\delta = 2$, and an extremely heavy-tail. This suggests that the heavy-tail portion unaccounted for by the two-flow model is in fact contributed by busy sources with large numbers of concurrent connections. However, the accuracy of the 10-flow model is only weakly justified.

## 5. Results

We now use our source model in our modeling framework to study the performance of Robust Header Compression schemes defined by a set of parameters $\{\Psi^K, w, r\}$. Using both analysis and simulation, we evaluate the performance of current ROHC-TCP specifications under different source and deployment scenarios. We then compare the performance of optimized codebooks with and without intermediate encoding, benchmarked against the (unoptimized) ROHC performance. Using numerical examples, we illustrate the concept of tradeoff optimization at the desired level of performance. The optimized schemes obtained are then used in the performance tradeoff study. To illustrate the usefulness and flexibility of our framework and source model, our study involves *different* source scenarios and *different* deployment scenarios.

Three source scenarios are studied: the non-concurrent source (one-flow model) representing an idealized source, an average source (two-flow model) or a busy source (10-flow model). We also study different deployment scenarios by varying the Channel A and Channel B models, examining the scenario of source-compressor co-location (perfect Channel A) or non co-location (wireless Channel A). Channel B deployment scenarios are varied at high speed or low speed mobility in wireless Channel B. We study encoding variations based on whether the WLSB codebook is directly applied on uncompressed fields, or with INFERRED-OFFSET as a prior intermediate step.

Table 3
Channel model parameters

| | Low speed (2 km/h) | High speed (50 km/h) |
|---|---|---|
| $P_{gb}$ | $1.67 \times 10^{-5}$ | $5.35 \times 10^{-5}$ |
| $P_{bg}$ | $1.66 \times 10^{-3}$ | $4.96 \times 10^{-4}$ |
| $\mathrm{BER_g}$ | $10^{-5}$ | $10^{-5}$ |
| $\mathrm{BER_b}$ | 0.1 | 0.1 |

Table 4
Current ROHC-TCP specifications

| Parameter | Specification |
|---|---|
| IPID WLSB codebook, $\Psi^K$ | $\{(0,0),(6,0),(8,0),(11,1),(12,1),16\}$, with intermediate encoding using MSN |
| Context window size, $w$ | Up to implementation |
| Context refresh period, $r$ | Up to implementation |

Using results from literature [21], two sets of parameters are used to model different mobility speeds as shown in Table 3. We set the uncompressed packet size to 300 bytes (in Channel A) and compressed packet size to 265 bytes (in Channel B). This comes from the fact that the mean size of data packets is near 300 bytes in the trace, and that header compression typically reduces the 40 bytes TCP/IP header to 5 bytes.[1]

Table 4 shows an extract from the current ROHC specifications for compressing TCP/IP headers (ROHC-TCP). Note that the WLSB offset parameter, $o_f$, changes from 0 to 1 for the third and fourth code in the codebook. This change is made to accommodate the case of single packet re-ordering in either Channel A or Channel B. Since this change has almost no effect on the interpretation intervals, and our channel processes do not model packet re-ordering, we use a constant $o_f = 0$ in our study. Note also that the context window size and context refresh period are left as implementation parameters with unspecified values in ROHC. We will illustrate the process of obtaining tradeoff optimized values for these parameters.

Using our modeling framework and source models, we obtain numerical values for the three performance metrics. We verify our framework by comparing the results from the average source model with those from trace-based simulation. To do this, we obtained a separate trace, TCP180903out, consisting of 285,571 packets captured over a half-hour interval on a *different* day from the previous trace.

Fig. 16 depicts the encoding performance of ROHC-TCP specifications under the three source types (non-concurrent, average and busy) and the two Channel A types (perfect or wireless). This is measured using the inverse of the asymptotic ($r \to \infty$) Compression Efficiency, $1/\mathrm{CE}_\infty$, which gives the ratio of the asymptotic mean compressed length over the uncompressed length (see Eq. (29)). Naturally, smaller ratios are indicative of higher compression efficiency and better performance. We first note that the performance obtained from trace-based simulation agree well with analytical results from the average source model, which was built from a different trace. Second, we observe that the compression efficiency is dependent on the nature of the source scenario and Channel A. A busier source deteriorates the compression efficiency, and packet drops in Channel A cause further degradation of performance, though to a lesser extent. Note in particular that the idealized operating environment of non-concurrent source with perfect Channel A gives unrealistically good and constant performance regardless of the context window size, which is far from actual cases found in real world. Thus, over-optimistic conclusions drawn from performance evaluations making this assumption might inadvertently prompt implementations to use large context window sizes for high robustness without clear understanding of its tradeoffs. Third, with the exception of the aforementioned case, the compression efficiency generally decreases with increasing context window size (robustness). This agrees with intuition that there is tradeoff involved between compression efficiency and robustness.

Examine next Fig. 17, which shows the compression transparencies, CT, over wireless Channel B at two different extents of mobility, after compression using the ROHC codebook. Each single curve denotes a fixed

[1] These are based on data payloads. Per packet gains from real-time applications like Voice over IP (VoIP) are typically much higher due to smaller payloads.

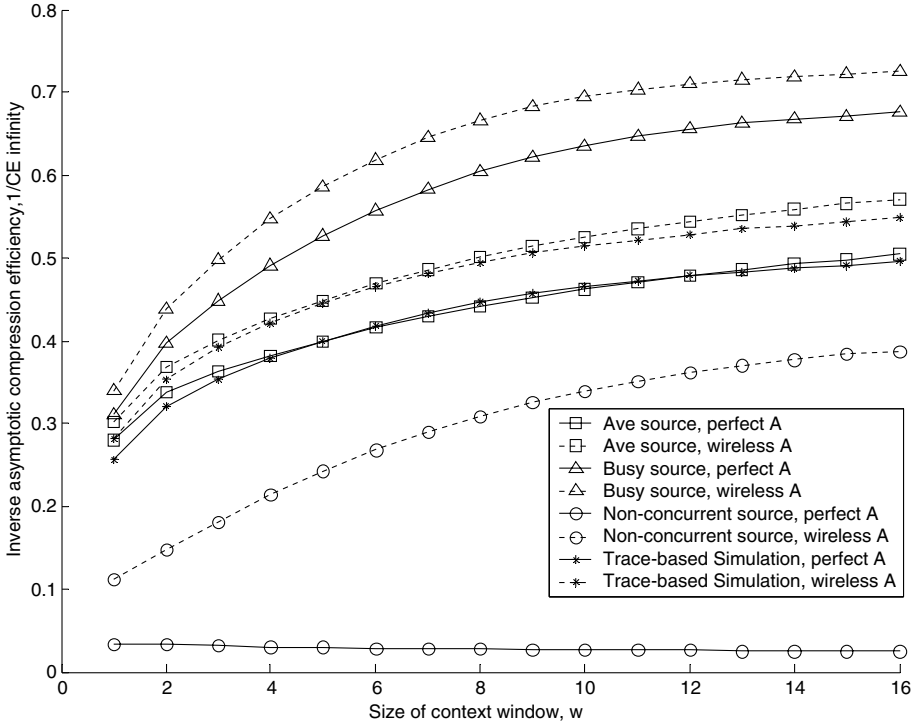


Fig. 16. The encoding performance of ROHC-TCP IPID codebook in the face of various source and Channel A types. The plot shows the inverse of the asymptotic compression efficiency, $1/CE_{\infty}$ versus the context window size, $w$. $1/CE_{\infty}$ is a ratio of the asymptotic mean compressed length over the uncompressed length. The context window size is also a measure of robustness.

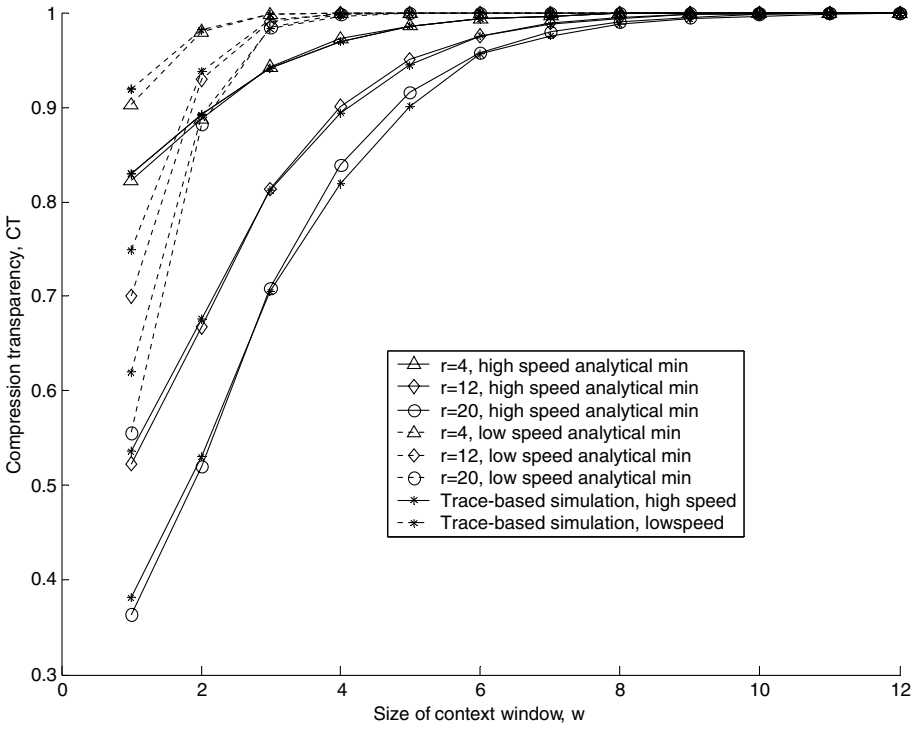


Fig. 17. Compression transparency in wireless Channel B versus context window size at high speed or low speed mobility. The compression transparency, CT, is almost identical to the minimum compression transparency, $CT_{min}$.

context refresh period, $r$. We observe that for each fixed $r$, the CT curve obtained from trace-based simulation is mostly close to and above the analytical $CT_{min}$ bound. It is clear from Fig. 17 that CT can be increased by increasing the context window size to improve the robustness of the scheme. However, the choice of $(w,r)$ parameters depends greatly on the extent of mobility in wireless Channel B. Evidently, high speed mobility requires greater robustness in terms of higher $w$ values and/or more frequent context refreshes (lower $r$ values) to achieve the same compression transparency. The significance of this is that these two parameters should be made adaptive if the extent of node mobility is not expected to be fixed in deployment scenarios.

The following results demonstrate the three steps involved in our optimization procedure in Section 3.7.2. Applying Step 1 of our optimization procedure, we examine the asymptotic compression efficiencies of optimized codebooks $\Psi_{\text{opt}}^{K_{\text{opt}}}(w)$ using (i) direct WLSB encoding and (ii) with intermediate encoding using the MSN field. Both data sets are benchmarked against the (unoptimized) ROHC codebook in Fig. 18. The case of an average source and perfect Channel A is assumed. As expected, the use of prior offset against the MSN field, as prescribed in ROHC-TCP, increases the compression efficiency. We note that the optimized codebook is non-constant and may change incrementally as $w$ increases. On the other hand, the ROHC codebook remains constant for all context window size $w$, and it can be seen that its asymptotic compression efficiencies fall below that from the optimum codebook at all $w$. In the range $w \geqslant 3$, the ROHC codebook is not far from optimum. Therefore, the ROHC codebook may be used as a reasonable approximation to $\Psi_{\text{opt}}^{K_{\text{opt}}}$, which is constant for all $w$. It will be demonstrated later how the remaining two parameters $w_{\text{opt}}$ and $r_{\text{opt}}$ in the optimized scheme $\{\Psi_{\text{opt}}^{K_{\text{opt}}}(w_{\text{opt}}), w_{\text{opt}}, r_{\text{opt}}\}$ may be found.

We examine the reason for the compression efficiency improvement due to intermediate encoding in Fig. 19, which compares the IPID delta cumulative distributions for the two encoding variations on a log scale. Notice the key difference that the set of distributions with intermediate encoding starts from non-zero probabilities at the vertical axis where $b = 0$. This allows WLSB encoded fields to be efficiently encoded into *zero bits* (i.e. which is also known as STATIC encoding) with significant probabilities, lowering the mean encoded size. The choice of the MSN field as the offset base field achieves this remarkably well as it shares the incrementing characteristic with the IPID field.

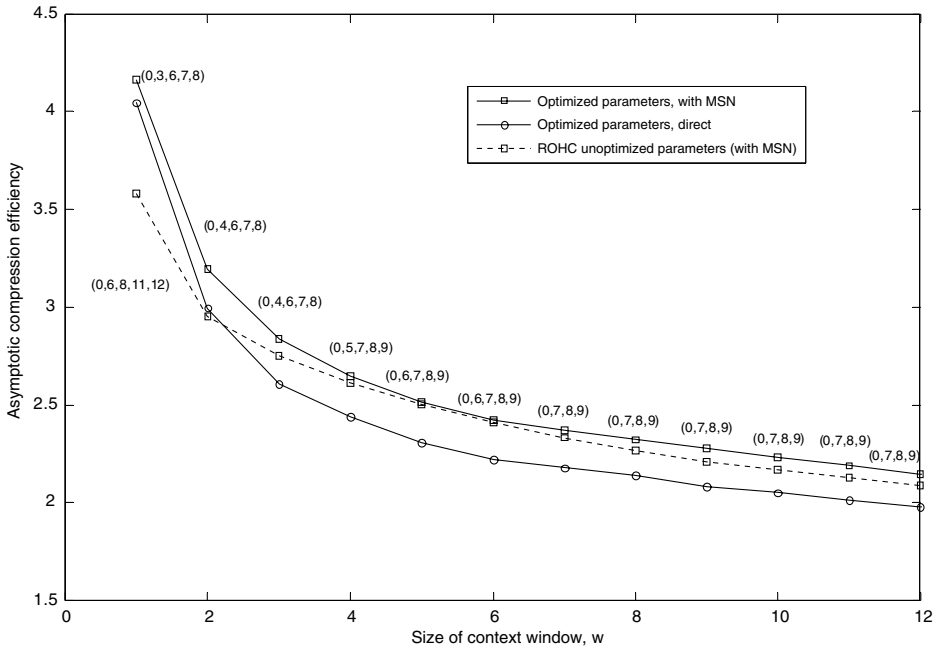


Fig. 18. Asymptotic compression efficiencies of optimized codebooks for direct WLSB encoding compared to WLSB with prior offset against the MSN. This is benchmarked against the ROHC codebook. The case of the average source with perfect Channel A is assumed. The set of $b$-parameters $\{b_i\}_{i=1}^{K-1}$ is shown as a vector for each point.

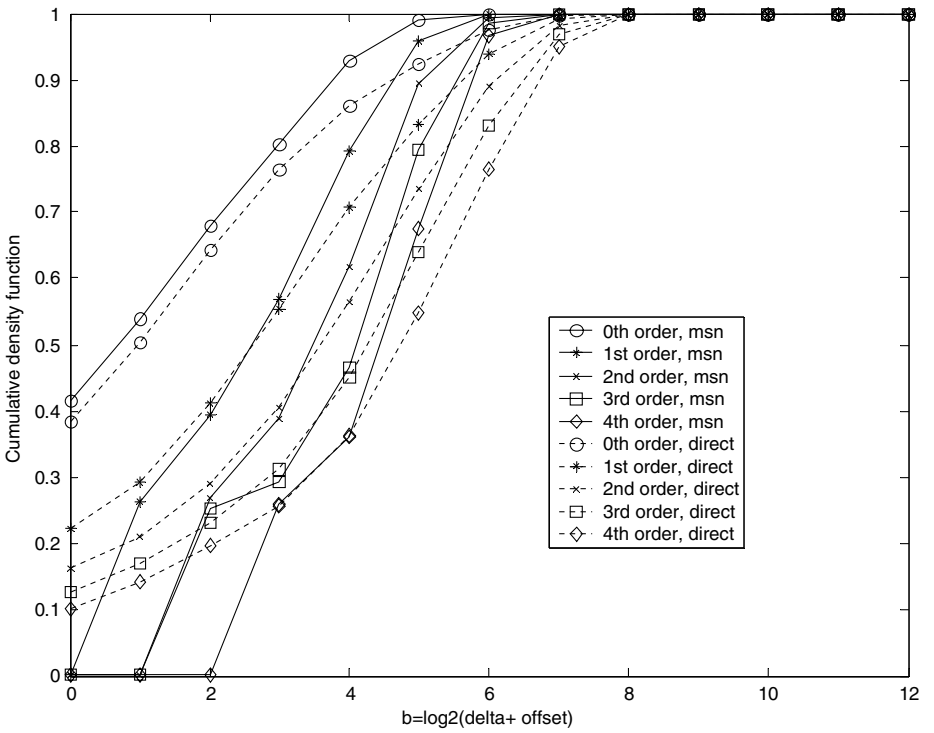


Fig. 19. IPID delta cumulative distribution at high orders, without intermediate encoding (direct), compared to that with intermediate encoding (MSN).

We now illustrate the concept of meeting the desired level of compression transparency guarantee $\mathrm{CT}_{\mathrm{des}}$ using $\mathrm{CT}_{\mathrm{min}}$. Fig. 20 shows two sets of $\mathrm{CT}_{\mathrm{min}}$ curves, at high speed and low speed mobility in wireless Channel B. The context refresh period, $r$ is fixed in each single curve. We observe that higher context refresh periods result in lower $\mathrm{CT}_{\mathrm{min}}$ curves. A horizontal line is drawn at *desired* $\mathrm{CT}_{\mathrm{min}} = \mathrm{CT}_{\mathrm{des}} = 0.96$ as an example of indicating the desired level of (minimum compression transparency) performance. Given the extent of Channel B mobility, the points above the line form the set of $(w,r)$ combinations guaranteeing that level of compression transparency. In Step 2 of our optimization procedure, all combination pairs satisfying this criterion are put into the set $\zeta$.

Having obtained the set of $(w,r)$ combination pairs providing transparency guarantee (for a given channel mobility), the next question arises on *which* is the *best pair* to use. This is determined by choosing the pair with the highest compression efficiency in Step 3 of the optimization procedure. We now consider the spectrum of CE curves for the case of average source and perfect Channel A in Fig. 21. We note that the asymptotic compression efficiency, $\mathrm{CE}_{\infty}$ is the highest curve at which $r \to \infty$. A horizontal *desired* $\mathrm{CT}_{\mathrm{min}}$ line in Fig. 20 indicating the desired level of transparency transforms into a dotted curve in Fig. 21. Agreeing with intuition, curves at higher transparencies suffer slides in compression efficiencies. Another result is that the *same desired level of transparency* is achieved at different compression efficiencies depending on the extent of mobility in wireless Channel B. Finally, the optimum set of parameters $\{\Psi_{\mathrm{opt}}^{K_{\mathrm{opt}}}(w_{\mathrm{opt}}), w_{\mathrm{opt}}, r_{\mathrm{opt}}\}$ at the desired level of transparency $\mathrm{CT}_{\mathrm{min}}$ can be found at the maxima of the *desired* $\mathrm{CT}_{\mathrm{min}}$ dotted curve in Fig. 21. For example, suppose $\mathrm{CT}_{\mathrm{des}} = 0.96$ in high speed mobility. In this case, the optimum $(w,r)$ pair, $(w_{\mathrm{opt}}, r_{\mathrm{opt}}) = (7,48)$, can be found at the maxima of the $\mathrm{CT}_{\mathrm{min}} = 0.96$ curve for high speed mobility as shown in Fig. 21. Since $w_{\mathrm{opt}}$ is known, the optimum codebook $\Psi_{\mathrm{opt}}^{K_{\mathrm{opt}}}(w_{\mathrm{opt}})$ for this scenario is obtained by referring to Fig. 18, i.e. $\Psi^{K_{\mathrm{opt}}}(w_{\mathrm{opt}}) = \{(0,0),(7,0),(8,0),(9,0),16\}$.

Fig. 22 shows the tradeoff involved between the optimum compression efficiencies (from optimized schemes) and the desired levels of minimum compression transparency. Note that we have not shown the non-concurrent source results in Fig. 22 because it is simply a horizontal line at $\mathrm{CE}_{\infty} = 40$, which is out of

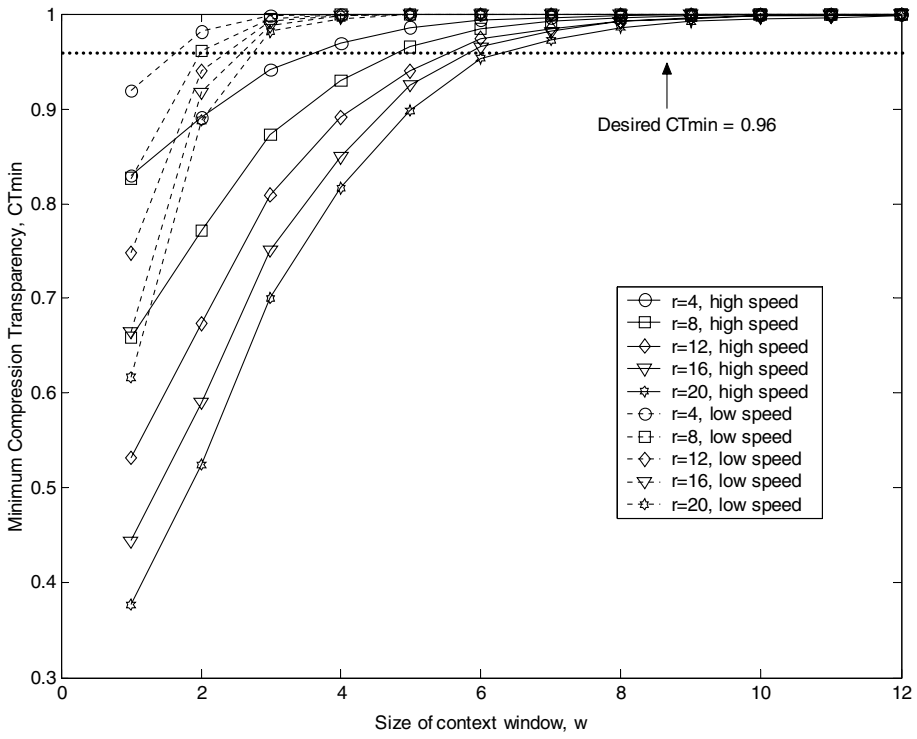


Fig. 20. Variation of minimum compression transparency, $CT_{min}$ with context window size or robustness, $w$.

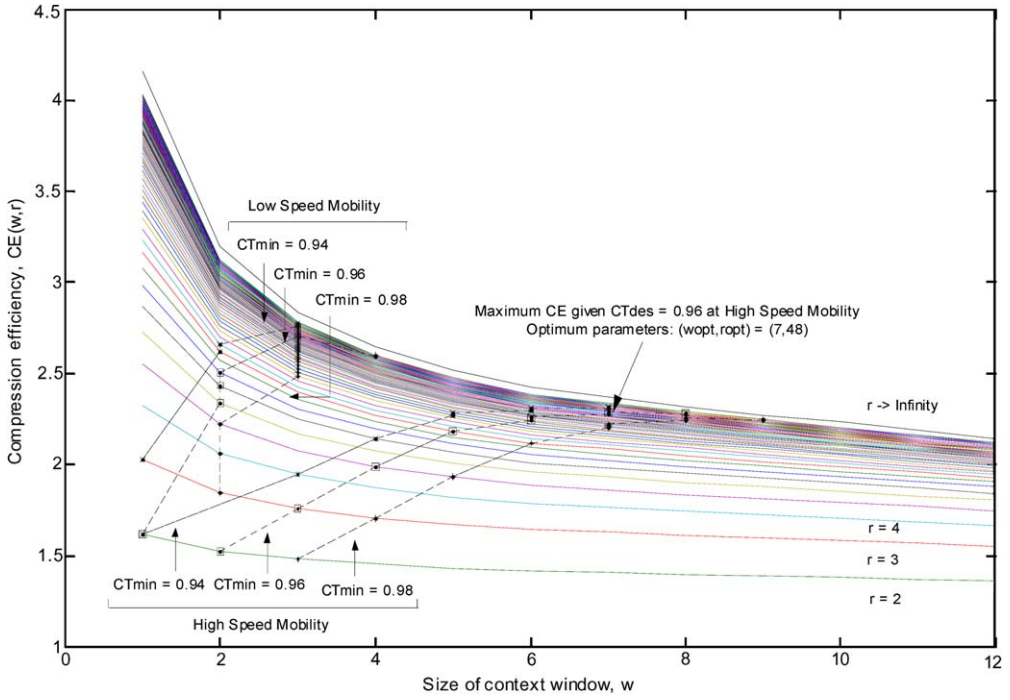


Fig. 21. Compression efficiencies, CE at various context window size, $w$ and context refresh periods, $r$ for the average source and perfect Channel A.

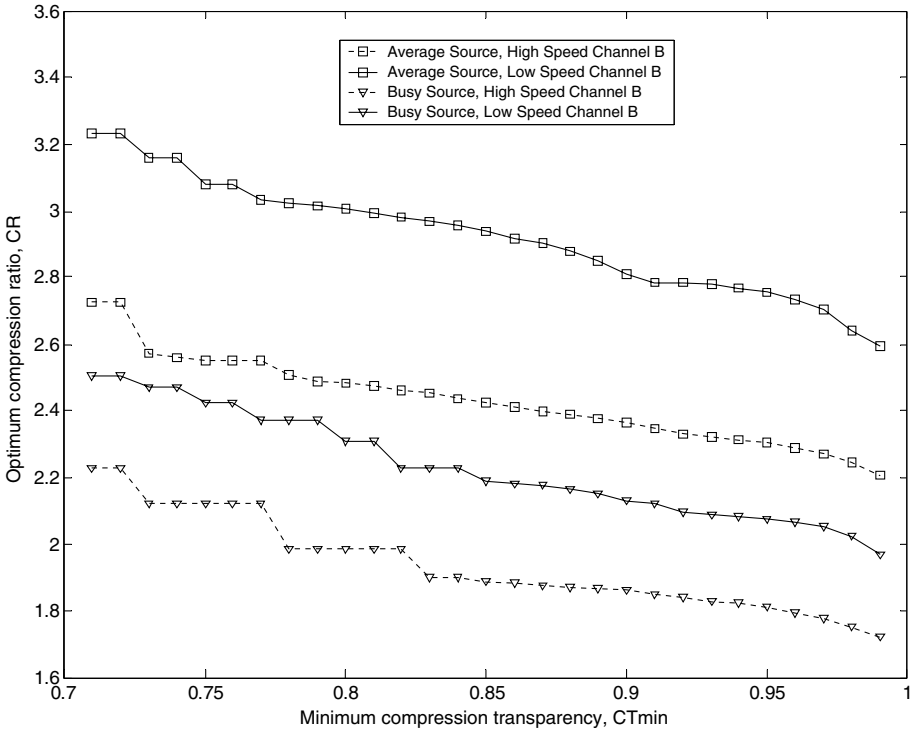


Fig. 22. Variation of optimum compression efficiencies with the desired minimum compression transparency, showing the tradeoffs involved.

scale. Otherwise, due to relatively gentle slopes, we note that the compression transparency improves greatly with relatively little sacrifice in compression efficiency. This is good news for optimized robust schemes. We can see that the tradeoff curve obtained is heavily dependent on the nature of the source and extent of mobility in Channel B. Thus, the effects of different source and deployment scenarios on header compression are too significant to be ignored.

## 6. Future work

By proposing our source model, we have taken the first step towards the modeling of real-world operating environments. We acknowledge that the current source model requires further work for improvement. Future work involves extending the source model to cover multiple CHANGING fields with inter-dependency, and the development of a more accurate model with a non-constant number of concurrent flows.

We have also opened up the possibility of performing adaptive scheme optimization. Though we have demonstrated scheme optimization using the source model in this paper, the source model is not mandatory for this purpose. A header compression system in deployment can also use its trace sequence to compute performance metrics online, based on which it can adaptively optimize its parameters following the principles developed in this paper.

## 7. Conclusion

We have presented some novel contributions in this paper. For the first time, a source model has been developed for studying header compression. Since it also models the way packets are generated from a source handling multiple concurrent flows, the source model can also be used for more general applications. We have presented a modeling framework allowing the study of header compression performance in different scenarios. Using our framework, we have offered new perspectives to the definition of performance metrics and studied

tradeoffs in a novel way. We have shown for the first time that header compression schemes can be optimized at desired levels of performance. Our results reveal that the common assumption of non-concurrent sources and perfect Channel A leads to over-optimistic performance evaluations. Finally, we have shown that achieved performance and tradeoffs are heavily dependent on the source and deployment scenarios, and these should not be ignored in both scheme design and performance evaluation.

## Appendix A. Derivation of Eq. (45)

When $N = 2$, we know from Eq. (33) that there are only two paths out of each state. For any $\delta$ in $P(\Delta = \delta|\mathscr{S} = (f_o, i))$, the first $\delta - 1$ transitions must occur to a state outside the flow of observation, $f_o$; the last transition is back to $f_o$. Because there is only a single flow outside $f_o$, there is only a single deterministic path to follow. For $\delta = 1$, the result of Eq. (42) remains unchanged. For $\delta \geqslant 2$, using the same logic for evaluating $P(\Delta = \delta|\mathscr{S} = (f_o, i))$ in Section 4.1, it is straightforward to obtain the following expression by following the deterministic path:

$$P(\Delta = \delta|\mathscr{S} = (f_o, i)) = (1 - q_{(f_o,i)}^{(f_o,i+1)})Q(f_1, \delta - 2)(1 - q_{(f_1,\delta-1)}^{(f_1,\delta)}). \tag{A.1}$$

Substituting into Eq. (38), we have for $N = 2$ and $\delta \geqslant 2$

$$\begin{aligned} P(\Delta = \delta) &= \frac{p(f_o, 1)}{p(f_o)} \left[ \sum_{i=1}^{\infty} Q(f_o, i-1)(1 - q_{(f_o,i)}^{(f_o,i+1)}) \right] \times Q(f_1, \delta - 2)(1 - q_{(f_1,\delta-1)}^{(f_1,\delta)}), \\ &= \frac{p(f_o, 1)Q(f, \delta - 2)(1 - q_{(f_1,\delta-1)}^{(f_1,\delta)})}{p(f_o)}, \quad \delta \geqslant 2. \end{aligned} \tag{A.2}$$

The expression inside the square parentheses of the above expression is shown to be 1

$$\left[ \sum_{i=1}^{\infty} Q(f_o, i-1)\left(1 - q_{(f_o,i)}^{(f_o,i+1)}\right) \right] = 1. \tag{A.3}$$

**Proof**

$$\begin{aligned} \sum_{i=1}^{\infty} Q(f_o, i-1)(1 - q_{(f_o,i)}^{(f_o,i+1)}) &= \sum_{i=1}^{\infty} Q(f_o, i-1) - \sum_{i=1}^{\infty} Q(f_o, i) = 1 + \sum_{i=2}^{\infty} Q(f_o, i-1) - \sum_{i=1}^{\infty} Q(f_o, i) \\ &= 1 + \sum_{i'=1}^{\infty} Q(f_o, i') - \sum_{i=1}^{\infty} Q(f_o, i), \quad \text{where } i' = i - 1, \\ &= 1. \qquad \square \end{aligned}$$

## Appendix B. Derivation of Eq. (47)

The $n$th order delta probability at steady state can be expressed as a fraction of $n$th and $(n-1)$th order joint probabilities

$$\gamma_n = \frac{\hat{P}(\Delta(n_A) = 1, \ldots, \Delta(n_A - n) = 1)}{\hat{P}(\Delta(n_A) = 1, \ldots, \Delta(n_A - (n-1)) = 1)}. \tag{B.1}$$

Consider first the approximated model with infinite states per flow. We can then find the expression for *any* $n$th order joint probability as

$$\hat{P}(\Delta(n_A)=1,\ldots,\Delta(n_A-n)=1)=\frac{1}{P(f_o)}\left[P(f_o,1)\prod_{i=1}^{n+1}q_{(f_o,i)}^{(f_o,i+1)}+P(f_o,2)\prod_{i=2}^{n+2}q_{(f_o,i)}^{(f_o,i+1)}+\ldots\right]$$
$$=\frac{P(f_o,1)}{P(f_o)}\left[\sum_{j=1}^{\infty}\prod_{i=1}^{n+j}q_{(f_o,i)}^{(f_o,i+1)}\right]. \tag{B.2}$$

A fraction of the $n$th and $(n-1)$th order joint probabilities would yield

$$\frac{\hat{P}(\Delta(n_A)=1,\ldots,\Delta(n_A-n)=1)}{\hat{P}(\Delta(n_A)=1,\ldots,\Delta(n_A-(n-1))=1)}=\frac{\sum_{j=1}^{\infty}\prod_{i=1}^{n+j}q_{(f_o,i)}^{(f_o,i+1)}}{\sum_{j=1}^{\infty}\prod_{i=1}^{n+j-1}q_{(f_o,i)}^{(f_o,i+1)}}=\frac{\sum_{j=n+1}^{\infty}\prod_{i=n+1}^{j}q_{(f_o,i)}^{(f_o,i+1)}}{1+\sum_{j=n+1}^{\infty}\prod_{i=n+1}^{j}q_{(f_o,i)}^{(f_o,i+1)}}. \tag{B.3}$$

We now adapt Corollary 1 to a more general scenario required in Eq. (B.3) where mapping occurs from state $(f,n+1)$ onwards

$$\sum_{j=n+1}^{\infty}\prod_{i=n+1}^{j}q_{(f,i)}^{(f,i+1)}=\begin{cases}\sum_{j=n+1}^{h_f-1}\prod_{i=n+1}^{j}q_{(f,i)}^{(f,i+1)}+\frac{q_{(f,h_f)}^{(f,h_f)}}{1-q_{(f,h_f)}^{(f,h_f)}}\prod_{i=n+1}^{h_f-1}q_{(f,i)}^{(f,i+1)}, & 0\leqslant n\leqslant h_f-2,\\ \frac{q_{(f,h_f)}^{(f,h_f)}}{1-q_{(f,h_f)}^{(f,h_f)}}, & n\geqslant h_f-1.\end{cases} \tag{B.4}$$

Substituting Eq. (B.4) into Eq. (B.3) in the same form as Eq. (47) and noting that

$$\alpha_n=\begin{cases}\left(1-q_{(f_o,h_o)}^{(f_o,h_o)}\right)\sum_{j=n+1}^{h_o-1}\prod_{i=n+1}^{j}q_{(f_o,i)}^{(f_o,i+1)}\\ \quad+q_{(f_o,h_o)}^{(f_o,h_o)}\prod_{i=n+1}^{h_o-1}q_{(f_o,i)}^{(f_o,i+1)}, & 0\leqslant n\leqslant h_o-2,\\ q_{(f_o,h_o)}^{(f_o,h_o)}, & n\geqslant h_o-1.\end{cases} \tag{B.5}$$

we obtain Eq. (47).

## References


[1] V. Jacobson, Compressing TCP/IP headers for low-speed serial links, RFC 1144, 1990.
[2] C. Bormann et al., RObust Header Compression (ROHC): Framework and four profiles: RTP, UDP, ESP, and uncompressed, RFC 3095, July 2001.
[3] ROHC Charter. Available from: <http://www.ietf.org/html.charters/rohc-charter.html>.
[4] M. West, S. McCann, TCP/IP field behavior, internet draft (work in progress), <draft-ietf-rohc-tcp-field-behavior-02.txt>, March 2003.
[5] Pelletier, G., Zhang, Q., Jonsson, L-E., Liao, H., West, M., RObust Header Compression (ROHC): TCP/IP Profile (ROHC-TCP), Internet Draft (work in progress), <draft-ietf-rohc-tcp-07.txt>, 2004.
[6] R. Sridharan, R. Sridhar, S. Mishra, A robust header compression technique for wireless ad hoc networks, ACM SIGMOBILE'03 7 (3) (2003) 23–24.
[7] Effnet HC-SIM. Available from: <http://www.effnet.com/sites/effnet/pages/uk/products_hc-sim.asp>.
[8] Acticom ROHC evaluation tool. Available from: <http://www.acticom.de/1412.html>.
[9] H. Liao, Q. Zhang, W. Zhu, Y.-Q. Zhang, A robust TCP/IP header compression scheme for wireless networks, IEEE International Conference on 3G wireless and Beyond (3Gwireless'01), June 2001, San Francisco, CA, USA.
[10] M. Degermark, B. Nordgren, S. Pink, IP Header Compression, RFC 2507, February 1999.
[11] C. Perkins, J. Crowcroft, Effects of interleaving on RTP header compression, in: Proceedings of IEEE Infocom 2000, Tel Aviv, Israel, March 2000.
[12] P. Seeling, M. Reisslein, F.H.P. Fitzek, S. Hendrata, Video quality evaluation for wireless transmisison with robust header compression, in: Proceedings of the IEEE Fourth International Conference on Information, Communications & Signal Processing and Fourth IEEE Pacific-Rim Conference on Multimedia (ICICS-PCM 03), Singapore, pp. 1346–1350.
[13] X. Gu, H. Hartenstein, S. Fischer, A robust header compression simulator & visualizer, in: Proceedings of the International Conference on Architectures of Computing SystemsLecture Notes in Computer Science, vol. 2299, Springer, 2002, pp. 274–286.
[14] J. Ash, B. Goode, J. Hand, R. Zhang, Requirements for header compression over MPLS, Internet Draft (work in progress), <draft-ietf-avt-hc-mpls-reqs-02.txt>, June 2004.

[15] C.Y. Cho, S.K. Hazra, W.K.G. Seah, Exploiting inter-flow redundancy: context replication in ROHC-TCP, in: Proceedings of IEEE Global Telecommunications Conference (GLOBECOM 2004).
[16] H. Wang, K.G. Seah, An analytical model for the ROHC RTP profile, in: Proceedings of the IEEE Wireless Communications and Networking Conference 2004, WCNC 2004.
[17] C. Westphal, R. Koodli, IP Header compression: A study of context establishment, WCNC 2003—IEEE Wireless Communications and Networking Conference 4 (1) (2003) 1025–1031.
[18] C. Jiao, L. Schwiebert, G. Richard, Adaptive header compression for wireless networks, in: 26th Annual IEEE Conference on Local Computer Networks (LCN'01), November 2001, pp. 377.
[19] M. Menth, O. Rose, Performance tradeoffs for header compression in MPLS networks, in: Technical Report 291, University of Würzburg Institute of Computer Science Research Report Series, November 2001.
[20] C. Jiao, L. Schwiebert, B. Xu, On modeling the packet error statistics in bursty channels, in: 27th Annual IEEE Conference on Local Computer Networks (LCN'02), November 2002, pp. 534–541.
[21] P. Lettieri, C. Fragouli, M.B. Srivastava, Low power error control for wireless links, in: Proceedings of ACM/IEEE MobiCom'97, 1997, pp. 139–150.

**Chia Yuan Cho** received the B.Eng. degree with First Class Honors from the National University of Singapore in December 2003, supported by Singapore's Defence Science and Technology Agency (DSTA) scholarship. Selected into the University's Accelerated Masters Program, he completed his M.Eng. candidature in January 2005. He is currently a Member of Technical Staff at DSO National Laboratories, an affiliate of the Defence Science and Technology Agency. His current research interests include network security, network traffic modeling and wireless networks.

**Winston Khoon Guan Seah** received the Dr.Eng. degree from Kyoto University, Kyoto, Japan, in 1997. He is a Lead Scientist in the Networking Department of the Institute for Infocomm Research ($I^2R$). Prior to $I^2R$, he had been a Principal Member of Technical Staff, and director of the Internet Technologies programme in the Institute for Communications Research. He is an Adjunct Associate Professor in the School of Electrical and Electronic Engineering, Nanyang Technological University, Singapore. Concurrently, he is an adjunct faculty in the Graduate School for Integrative Science and Engineering, and the Department of Computer Science in the National University of Singapore where he lectures in mobile computing. He is actively involved in research and development in the areas of mobile ad hoc and sensor networks, co-developed one of the first quality of service (QoS) models for mobile ad hoc networks (MANET), and has given keynote talks on the area of QoS for MANETs. His latest research focuses on mobility-enhanced protocols and algorithms for $C^3$ and sensing applications in terrestrial and oceanographic ad hoc sensor networks. He is also on the TPC of numerous conferences and reviewer of papers for many key journals and conferences in the area of MANET and sensor networks. He serves on the Steering Committee of the Asia-Pacific IPv6 Task Force, and is also an associate of the Singapore Advanced Research and Education Network (SingAREN.) He is a Senior Member of the IEEE. [Homepage: http://www1.i2r.a-star.edu.sg/~winston]

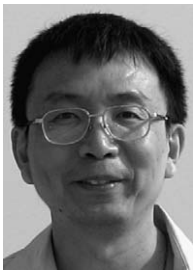

**Yong Huat Chew** received the B.Eng., M.Eng. and Ph.D. degrees in electrical engineering from National University of Singapore (NUS), Singapore. He has been with the Institute for Infocomm Research, an institute under Singapore Agency for Science, Technology and Research, since 1996, where he is presently a Lead Scientist. His research interests are in technologies towards high spectrally efficient wireless communication systems.